Applied Mathematical Modelling 39 (2015) 1137–1162

Contents lists available at ScienceDirect

Applied Mathematical Modelling

journal homepage: www.elsevier.com/locate/apm

Fatigue and static failure considerations using a topology optimization method

Seung Hyun Jeong [a], Dong-Hoon Choi [b], Gil Ho Yoon [b,*]

[a] Graduate School of Mechanical Engineering, Hanyang University, Republic of Korea
[b] School of Mechanical Engineering, Hanyang University, Republic of Korea

ARTICLE INFO

Article history:
Received 2 May 2013
Received in revised form 15 April 2014
Accepted 12 July 2014
Available online 10 August 2014

Keywords:
Topology optimization
Dynamic fatigue constraints
Gerber theory
Modified Goodman theory
Soderberg theory

ABSTRACT

We developed a new layout optimization method that incorporates dynamic fatigue and static failure criteria under constant and proportional mechanical loads. Although fatigue failure is one of the most important design considerations to ensure the safety of a mechanical structure, it has rarely been considered in terms of topology optimization due to several major theoretical and numerical difficulties. In addition to the numerical and theoretical issues associated with static failure criteria, we found that the local mode issue and the non-differentiability of the fatigue failure criteria needed to be addressed prior to performing fatigue constraint topology optimization. By resolving the inherent and newly-found issues associated with fatigue criteria, we were able to perform successful topology optimization with dynamic fatigue criteria under constant and proportional mechanical loads.

1. Introduction

In this study, we report the development of a novel fatigue constraint topology optimization (FCTO) method that considers dynamic failure criteria (fatigue) implemented using a stress-life approach under constant and proportional mechanical loading, as shown in Fig. 1. Since the introduction of topology optimization (TO) for a linear structure, TO has been applied to a wide range of engineering problems (see [1] and references therein). Nevertheless, the application of TO to dynamic failure constraints is regarded as one of the most difficult problems in engineering. Thus, despite some recent TO developments for static failure criteria, few studies have applied TO to dynamic fatigue failure [2–4]. To contribute to this important research topic, we investigate the application of dynamic failure theories and related issues in their implementation, and present a new and innovative FCTO procedure. In addition to the three well-known numerical difficulties and theoretical issues associated with the stress-based TO method (STOM), namely the singularity problem, the local constraint problem, and highly nonlinear behavior, the FCTO method has additional numerical issues not investigated prior to this research. First, we investigated the effect of the local mode problem of fatigue constraints, which requires static as well as harmonic analysis for the constant and proportional load shown in Fig. 1. If linear mass interpolation is used, a gradient-based optimizer cannot find a local optimum due to excessive oscillation of aggregated fatigue constraints, which results from the high stress value caused by the local mode problem. In addition, non-differentiable fatigue criteria constraints such as the modified Goodman, Soderberg, and Gerber criteria need to be relaxed for a successful FCTO method. As shown in Fig. 2, there are non-differentiable kinks associated with fatigue constraints based on the Soderberg and modified Goodman criteria. To effectively resolve these

* Corresponding author. Address: School of Mechanical Engineering, Hanyang University, Seoul, Republic of Korea.
E-mail addresses: gilho.yoon@gmail.com, ghy@hanyang.ac.kr (G.H. Yoon).

http://dx.doi.org/10.1016/j.apm.2014.07.020
0307-904X/

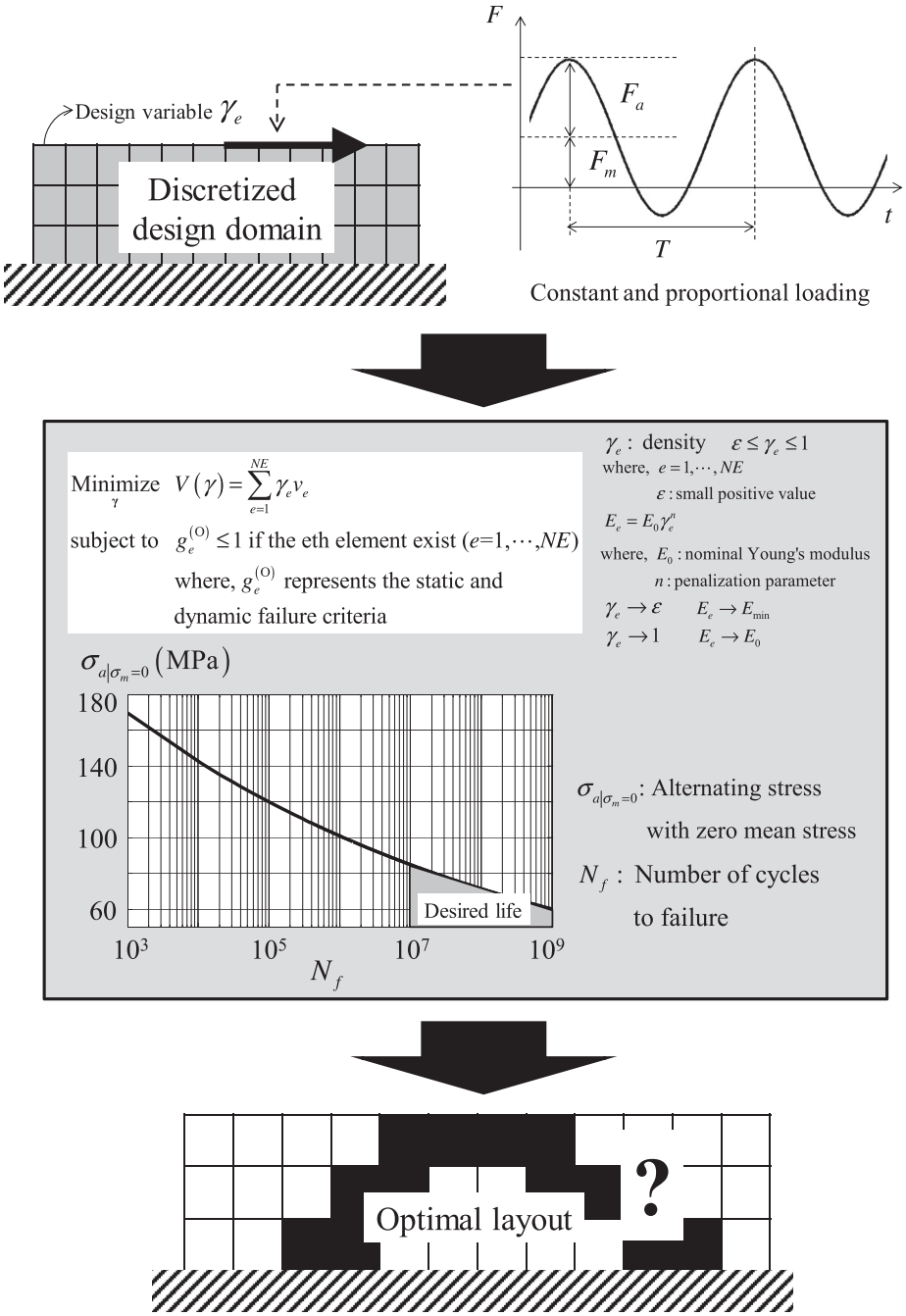

Fig. 1. Application of topology optimization with fatigue constraints.

additional issues, we proposed and implemented greater penalization of the element mass matrix with respect to the design variables and some differentiable relaxations for the non-differentiable criteria. In short, we successfully resolved new issues, including the local mode problem and non-differentiable criteria, for TO considering fatigue criteria.

1.1. Issues associated with fatigue constraint TO (FCTO)

Successful application of TO with fatigue constraints requires careful consideration of issues such as the local mode issue and the non-differentiability of constraints. TO was first formulated to minimize strain energy, i.e., compliance, subject to a volume constraint. Elaboration of this concept has led to application of TO to consider various kinds of static responses, dynamic responses, and even multiphysics system responses. Nowadays, TO approaches to minimize compliance subject

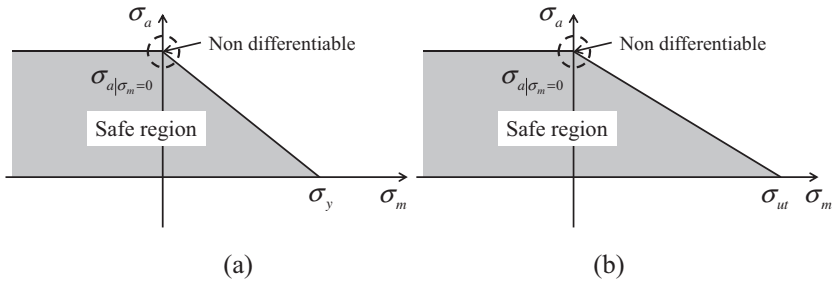

Fig. 2. Non-differentiable fatigue failure criteria: (a) Soderberg criterion and (b) modified Goodman criterion.

to a volume constraint and a compliant mechanism design are easily solved [1,5]. To optimize the response of a dynamic system, eigenvalue or dynamic responses can be considered directly [6]. Furthermore, it is now possible to optimize many multiphysics systems such as acoustic [7], electro-magnetic [8], and fluid–structure [9] environments by TO. Despite these applications of TO, local constrained structural TO taking static failure or dynamic failure into account remains one of the most difficult TO problems. There are three well-understood issues associated with TO with fatigue constraints: the singularity problem, the local constrained problem, and the highly nonlinear behavior [10–31] encountered in minimization of a volume subject to local von Mises stress constraints for a static load. The present TO method for dynamic fatigue is based on a stress-life approach with a static load and alternating load; several solutions to the difficulties and issues associated with the stress-based TO problem have been proposed. First, many solutions have been proposed to the singularity issue, [14,17,19,21–23,32,33]. Specifically, this issue occurs due to the material interpolation approach of the SIMP method which relaxes discrete design variables, i.e., zeros (voids) or ones (solids), so that these fall within a continuous variable range from a small positive value, i.e., 0.001 or 0.0001, to one. Although the stress values of finite elements for a void region should be zero, they often have non-zero values because small positive values are assigned to the corresponding design variables to represent a void region. Therefore, gradient-based optimization will be affected by a non-smooth optimization history. To resolve this singularity issue, the epsilon relaxation method [21,32], *qp*-relaxation method [16], and relaxed stress-indicator method [14,34] have been proposed. The *qp*-relaxation method and the relaxed stress-indicator share some similarities in terms of formulation of different penalization parameters for Young's moduli, and a constitutive matrix for stress evaluation is employed by both methods. Second, a local constraint issue arises because stress constraints are one of the local responses of a static system and the stress values of every center point of the finite elements should be constrained. Commonly, a gradient-based optimizer such as SQP (Sequential Quadratic Programming), SLP (Sequential Linear Programming), or MMA (Method of Moving Asymptotes) [35] benefits from a dual sub-problem formulation fit for optimization problems with a large number of design variables and a relatively small number of constraints. If we consider stress constraints for every finite element (FE), the number of constraints becomes large. In this case, a dual optimizer does not offer benefits. To solve this issue, a global constraint approach with *p*-norm [12,14,34] or Kreisselmeier–Steinhauser (KS) [10,12,13] has been proposed. In this global stress approach, an optimization problem with many local constraints can be transformed into an approximated optimization problem with a few global constraints that sufficiently approximate the local constraints. This global stress approach has been modified by dividing the design domain into several sub-domains to better account for the local behavior of the constraints [10,13,14,34]. Third, the highly non-linear behavior of stress constraints becomes an issue when design variables are relaxed and the global constraint approach is employed [11]. To resolve this issue, an accurate and efficient dual optimizer should be employed. The present FCTO method is based on a stress-life approach that considers static and alternating structural loads. Therefore, numerical issues related to the stress-constrained TO problem for a static structural load are encountered, and numerical techniques developed for stress-constrained TO should be applied.

1.2. Localized mode problem in dynamic fatigue problems

The localized mode problem encountered when applying TO to dynamic responses, including eigenvalues, is observed in the FCTO method. To optimize dynamic responses, a mass matrix as well as a stiffness matrix shall be interpolated with respect to the density design variables (see [1,36–38] and references therein for issues related to the dynamic problem). The localized mode problem becomes severe in the FCTO method when computing stress values for alternating structural loads. Some regions with a relatively large mass to stiffness ratio vibrate easily, and the stress values of the corresponding regions can increase drastically. Consequently, stress constraints are violated even at regions with *qp* stress relaxation, and stable convergence cannot be achieved. To overcome this phenomenon, we increased penalization of the mass penalty factor; this aspect will be discussed in more detail in the numerical section.

1.3. Non-differentiability of fatigue failure criteria

As stated above, we used a stress-life approach for fatigue criteria for a simple alternating stress status. Because common mechanical materials often have higher strength for a compressive load than a tensile load, it is necessary to distinguish

regions subject to a tensile load from those subject to a compressive load. However, in the case of multi-axial structural loads, it is not easy to identify whether an applied load is tensile or compressive. Furthermore, for a static structural load in addition to an alternating harmonic load, an effective multiaxial stress measure, such as the sum of hydraulic stress, the signed von Mises, or the signed maximum absolute principal stress, should be defined before applying the stress-life method [39–43]. Many fatigue experiments reported to date have revealed that a compressive load has a smaller influence on fatigue life than a tensile load. Therefore, the signed von Mises criterion or the signed maximum absolute principal stress should be employed to determine the state of the stress components of interest, either under a compressive load or tensile load, based on the sign of the maximum absolute principal stress. This calculation procedure becomes problematic in structural optimization due to determination of the signs of the principal stress values as well as the non-differentiable conditions. After calculating the effective multiaxial stress, the fatigue life can be estimated by the modified Goodman or Soderberg criterion; however, these are non-differentiable with respect to the effective multiaxial stress. Note the existence of some kinks of the envelopes of the fatigue life criteria in Fig. 2. To eliminate these kinks, we developed approximated differentiable formulations of the envelopes.

This paper consists of three sections. In section one, we provided an overview of topology optimization with fatigue constraints. In the second section, we present detailed formulations of the TO method with fatigue constraints. Accumulated damage to a mechanical structure under static and alternating loads due to fatigue failure as well as static failure are considered, and detailed formulations are provided in connection with TO. In the third section, several illustrative design optimization examples, including a simple two-bar, cantilever beam, and C-shape bracket, are solved with fatigue failure constraints. In particular, we highlight the validity and limitations of our proposed fatigue-constrained TO method by comparing the results of two-bar size optimization and two-bar topology optimization. Concluding remarks are provided and future research topics are discussed in the final section.

2. Topology optimization formulation for static failure and dynamic fatigue failure

This section is devoted to the development of a new TO formulation that considers dynamic fatigue failure in the framework of the SIMP method. First, basic assumptions regarding external mechanical loads (or fatigue loads) in connection with fatigue assessment are made. Furthermore, we reformulate the fatigue analysis procedure based on the stress-life approach using mean stress, i.e., modified Goodman or Gerber criteria for TO. Then, we derive the sensitivity of the fatigue failure constraint with respect to the design variables. We also modify the non-differentiable fatigue criteria for stress components into differentiable criterion formulations.

2.1. Fatigue analysis under static and alternating loads

2.1.1. Basic dynamic fatigue assumptions: stress life approach for constant and proportional loads

To consider fatigue phenomena in TO, we adopt the stress-life approach established by numerous tests as one of the total life approaches. Furthermore, we evaluate stress values at the centers of finite elements for *constant* and *proportional* loads. The "constant" load condition implies that the corresponding loading is a variant of a sine wave with a single load ratio. Therefore, one set of FE stress results, i.e., static and dynamic FE analysis results, is required to calculate the alternating and mean stress values. The "proportional" load condition implies that even though the radius of Mohr's circle varies during cyclic loading, the orientation of the principal axes with respect to the loading axes remains fixed. This proportional load condition is essential as a fatigue failure phenomenon, because non-proportional loads are not well understood. Furthermore, depending on the approach used to predict the load cycle limit before failure, state-of-the-art approaches to explain fatigue phenomena of a mechanical structure can be divided into two categories: total life approaches and damage tolerant approaches [40–43]. In a total life approach, the total number of effective loading cycles is estimated approximately by considering the magnitude of the effective stress applied to a mechanical component. The number of effective loading cycles before fatigue failure with respect to the stress magnitude can be graphically represented in a S-N diagram, which can be obtained from engineering fatigue experiments [40–43]. In real engineering applications, the history of stress or strain induced by an external mechanical load is recorded to characterize the effective loading cycle and the S-N diagram is used to calculate the number of loading cycles remaining before fatigue failure. In contrast, in a damage tolerant approach, propagations of pre-existing fatigue flows from initial sizes into critical sizes are analyzed analytically (see [40,42,43] and references therein for more details). We focus on the stress life approach as one of the total life approaches to characterize high cycle fatigue life. We also assume that external loads are constant and proportional.

2.1.2. Finite element analysis: static and dynamic FE analyses

For fatigue life analysis, the magnitudes of the alternating stress and mean stress need to be calculated [39–43]. In this research, we calculate mean stress values by static finite element analysis and alternating stress values by harmonic finite element analysis.

Static analysis is conducted using the following equation:

$$\mathbf{K}\mathbf{U}_m = \mathbf{F}_m, \tag{1}$$

where $\mathbf{K}$, $\mathbf{F}_m$, and $\mathbf{U}_m$ denote the global stiffness matrix, mean force vector, and the corresponding displacement vector, respectively. Global stiffness matrix is constructed by assembling the eth element stiffness matrix, $\mathbf{k}_e$, as follows:

$$\mathbf{K} = \mathop{\mathbf{A}}_{e=1}^{NE} \mathbf{k}_e \text{ and } \mathbf{k}_e = \int_{v_e} \mathbf{B}^{\mathrm{T}}\mathbf{C}_e\mathbf{B}dv \quad (v_e : e\text{th element domain}). \tag{2}$$

Here, $\mathbf{C}_e$ and $\mathbf{B}$ represent the constitutive matrix and the strain–displacement matrix, respectively. According to the material penalization method in the SIMP method [1,5,14,34,44], the constitutive matrix of the eth element is interpolated by using the eth design variable, γ_e, as follows:

$$\mathbf{C}_e = f_E(\gamma_e)\mathbf{C}_0 = \gamma_e^n\mathbf{C}_0, \tag{3}$$

where f_E, $\mathbf{C}_0$, and n are the interpolation function of the constitutive matrix, constitutive matrix without penalization, and penalization parameter, respectively. In this research, we fix the penalization value to 3. Without a loss of generality, the mean stress vector can be calculated using the displacement vector from the static analysis as follows:

$$\boldsymbol{\sigma}_{m,e} = {}_S\mathbf{C}_e\mathbf{B}\mathbf{u}_{m,e}, \tag{4}$$

$${}_S\mathbf{C}_e = f_S(\gamma_e)\mathbf{C}_0 = \gamma_e^{n_s}\mathbf{C}_0, \tag{5}$$

where f_S and ${}_S\mathbf{C}_e$ are the interpolation function for stress and the constitutive matrix for stress evaluation, respectively. The mean stress and the mean displacements of the eth element are denoted by $\boldsymbol{\sigma}_{m,e}$ and $\mathbf{u}_{m,e}$, respectively. Note that the penalization parameter, n_s, for stress evaluation is different than that of the static analysis to avoid the singularity issue associated with stress-based topology optimization [14,16,34]. A generally accepted value of the penalization parameter for stress evaluation is 0.5 (see [14,16,34] for more details).

Harmonic finite element analysis is conducted as follows:

$$(\mathbf{K} - \omega^2\mathbf{M})\mathbf{U}_a = \mathbf{K}_a\mathbf{U}_a = \mathbf{F}_a, \tag{6}$$

where $\mathbf{M}$, $\mathbf{K}_a$, $\mathbf{F}_a$, and $\mathbf{U}_a$ represent the mass matrix, dynamic stiffness matrix, alternating force, and the corresponding displacement vector, respectively, for an exciting angular velocity, ω. The consistence mass matrix can be assembled as follows:

$$\mathbf{M} = \mathop{\mathbf{A}}_{e=1}^{NE} f_M(\gamma_e)\mathbf{m}_e = \mathop{\mathbf{A}}_{e=1}^{NE} \gamma_e^{n_m}\mathbf{m}_e \text{ and } \mathbf{m}_e = \int_{v_e} \rho\mathbf{N}^{\mathrm{T}}\mathbf{N}dv \quad (\rho : \text{nominal density}), \tag{7}$$

where the penalization parameter for the mass matrix interpolation is denoted by n_m and the shape function of the eth element is $\mathbf{N}$. The interpolation function for the mass matrix is denoted by f_M. The value of mass penalization is important to avoid the localized mode issue; we fix this at 4 [1]. Without a loss of generality, the alternating stress vector can be calculated using the displacement vector from the harmonic analysis as follows:

$$\boldsymbol{\sigma}_{a,e} = {}_S\mathbf{C}_e\mathbf{B}\mathbf{u}_{a,e}. \tag{8}$$

Fig. 3 shows the interpolation functions for Young's modulus, stress, and the mass matrix. If the value of mass interpolation, n_m, is smaller than the value of Young's modulus interpolation, n, the natural frequency of a localized region becomes small at the element with a small design variable. Due to this phenomenon, the localized region vibrates severely, resulting

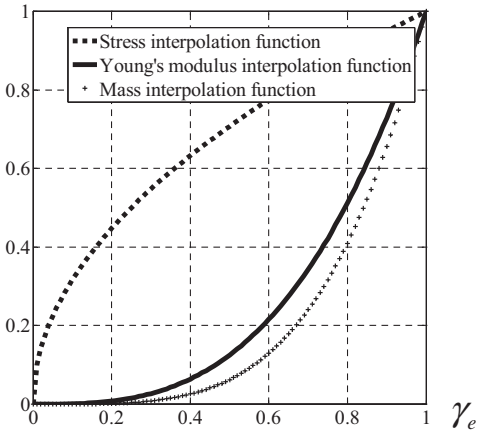

Fig. 3. Interpolation functions for Young's modulus, stress, and mass matrix.

in the local mode problem. If a large mass interpolation value is used, the local mode problem can be avoided because Young's modulus is larger than the mass for all density values, as shown in Fig. 3. Furthermore, the value of 0.5 for stress evaluation is important to avoid the singularity problem [14,21,34].

It is important to note that both static FE analysis (1) and harmonic FE analysis (6) are needed for fatigue analysis and the effective stress measures of the two FE analyses should be calculated to apply the S-N diagram obtained by the uniaxial fatigue test. After the mean and alternating stress components are calculated, the fatigue life can be estimated from the S-N diagram. Because the S-N diagram is generally obtained from a uniaxial fatigue cycle test, some measures are needed to represent the effect of multiaxial stress components. To do this, we employ the effective stresses approach [40–42].

2.2. Fatigue life approach: modified Goodman, Soderberg, and Gerber theories

We employ the modified Goodman, Gerber, and Soderberg theories in our TO of stress effects as follows:

$$\text{Modified Goodman}: \frac{\sigma_a}{\sigma_{a|\sigma_m=0}} + \frac{\max[\sigma_m, 0]}{\sigma_{TS}} \leqslant 1, \tag{9}$$

$$\text{Gerber}: \frac{\sigma_a}{\sigma_{a|\sigma_m=0}} + \left(\frac{\max[\sigma_m, 0]}{\sigma_{TS}}\right)^2 \leqslant 1, \tag{10}$$

$$\text{Soderberg}: \frac{\sigma_a}{\sigma_{a|\sigma_m=0}} + \frac{\max[\sigma_m, 0]}{\sigma_{y}} \leqslant 1, \tag{11}$$

where $\sigma_{a|\sigma_m=0}$, σ_y, and σ_{TS} represent the stress amplitudes for a fixed life for a completely reversed loading, yield strength, and tensile strength of the material of interest, respectively. Effective alternating and mean stresses are denoted by σ_a and σ_m, respectively. Many relevant measures and engineering theories based on numerous tests exist to effectively correlate the S-N diagram obtained by a one-dimensional uniaxial fatigue experiment (completely reversed stress cycles) with fatigue phenomena for a multi-axial mechanical load. The most popular criteria to apply the experiment results and observations from uniaxial load tests to failures with multiaxial loads are the Tresca, von Mises, and signed von Mises criteria. In this research, we use the signed von Mises measure as the effective stress measure for multi-axial mean stress because it can simultaneously consider tensile and compressive stress effects as well as the nominal magnitudes of stress components. Signed von Mises measure is explained later in his section while the others measures are described in the Appendix A [40–43]. Note that in Eqs. (9)–(11), the effect of the compressive effective mean stress is ignored by choosing a maximum value between zero and the employed mean stress measure (σ_m). Therefore, the effective mean stress measure should be formulated to consider the effect of compressive or tensile stress. To do this, we employ the signed von Mises criterion. However, the effective alternating stress measure is always positive because the magnitude of the fluctuating stress is considered. Therefore, we use the von Mises stress measure to represent the effective alternating stress as follows:

$$\sigma_a = \frac{1}{\sqrt{2}}\sqrt{(\sigma_{1a} - \sigma_{2a})^2 + (\sigma_{2a} - \sigma_{3a})^2 + (\sigma_{3a} - \sigma_{1a})^2}, \tag{12}$$

where σ_{1a}, σ_{2a}, and σ_{3a} are the sorted alternating principal stresses.

2.3. Multiaxial mean stress effect measure

Fatigue theories based on the results of fatigue uniaxial experiments have indicated that the effect of compressive mean stress can be negligible compared to the tensile mean stress. Therefore, from a computational point of view, it is important to determine whether a mechanical component of interest is under a compressive or tensile load [40–43]. For the case of a multiaxial load, this is not a trivial determination as with a uniaxial load case. In other words, it is challenging to determine whether an applied stress is compressive or tensile using a mean stress measure like the von Mises stress equivalent stress, because this measure is always positive. To determine whether an applied stress state is compressive or tensile, the sign of the maximum absolute principal stress component can be used for the signed von Mises criterion as follows [41]:

$$\sigma_m^{\text{signed von Mises}} = \begin{cases} \sigma_m^{\text{von Mises}} = \frac{1}{\sqrt{2}}\sqrt{(\sigma_{1m} - \sigma_{2m})^2 + (\sigma_{2m} - \sigma_{3m})^2 + (\sigma_{3m} - \sigma_{1m})^2} & \text{if } |\sigma_{1,m}| \geqslant |\sigma_{3,m}|, \\ -\sigma_m^{\text{von Mises}} = -\frac{1}{\sqrt{2}}\sqrt{(\sigma_{1m} - \sigma_{2m})^2 + (\sigma_{2m} - \sigma_{3m})^2 + (\sigma_{3m} - \sigma_{1m})^2} & \text{if } |\sigma_{3,m}| > |\sigma_{1,m}|. \end{cases} \tag{13}$$

Here, σ_{1m}, σ_{2m}, and σ_{3m} are the sorted mean principal stresses. It should be emphasized that the above criterion is not differentiable with respect to the stress components. Furthermore, due to its non-differentiability, it is impossible to adopt a gradient optimization algorithm such as SLP (Sequential Linear Programming), SQP (Sequential Quadratic Programming), or MMA (Method of Moving Asymptotes).

2.4. Topology optimization formulation considering fatigue failure

2.4.1. A new topology optimization formulation

Based on the basic assumptions for dynamic fatigue described above, we propose the following TO formulation that minimizes mass usage subject to fatigue failure constraints.

$$\begin{aligned} \underset{\boldsymbol{\gamma}}{\text{Minimize}} \quad & V(\boldsymbol{\gamma}), \\ \text{subject to} \quad & f_{1,e} = L_e^{(\odot)}(\sigma_a, \sigma_m) \leqslant 1, \\ & f_{2,e} = \frac{\sigma_{\max}}{\sigma_y} = \frac{\sigma_a + \sigma_m}{\sigma_y} \leqslant 1, \\ & f_{3,e} = -\frac{\sigma_{\min}}{\sigma_y} = \frac{\sigma_a - \sigma_m}{\sigma_y} \leqslant 1, \\ & \varepsilon \leqslant \gamma_e \leqslant 1, \quad e = 1, 2, \ldots, NE, \\ & \odot : \text{Fatigue criteria}(\text{Modified Goodman}, \ \text{Soderberg}, \ \text{Gerber}). \end{aligned} \tag{14}$$

Here, $\boldsymbol{\gamma}$ is the density design variable vector of the SIMP method for NE finite elements. The first constraint, $f_{1,e}$ or $L_e^{(\odot)}$, is the fatigue life constraint among the modified Goodman, Soderberg, and Gerber criteria of the eth finite element, which is a function of the alternating stress, σ_a, and the mean stress, σ_m. The superscript $\odot$ indicates the type of fatigue criteria among the modified Goodman, Gerber, and Soderberg criteria. To prevent static failure, referred to as one-time loading failure, the maximum absolute value of the sum of the alternating stress and the mean stress should be less than the yield strength at the second constraint, $f_{2,e}$, and the third constraint, $f_{3,e}$. The failure envelopes of the optimization problem using the fatigue failure criteria of Eqs. (9)–(11) and the constraint functions of Eq. (14) are represented in Fig. 4. When constraining the Soderberg criterion, the second constraint, $f_{2,e}$, can be ignored because the failure envelope belongs to that of the second constraint. Therefore, we only consider the modified Goodman and Gerber theories.

Singularity, local constraint, and highly nonlinear behavior issues associated with static stress-based topology optimization arise when dynamic and static stress constraints are defined at every finite element [10,14,15,22,34]. Therefore, we reformulate the original optimization problem in Eq. (14) by adopting a density filter method and global constraint approach as follows [14,34]:

$$\begin{aligned} \underset{\boldsymbol{\gamma}}{\text{Minimize}} \quad & V(\boldsymbol{\gamma}) = \sum_{e=1}^{NE} \tilde{\gamma}_e v_e, && (\tilde{\boldsymbol{\gamma}} : \text{Filtered density}) \\ \text{subject to} \quad & \langle f_{1,\max} \rangle_k \leqslant 1, \\ & \langle f_{2,\max} \rangle_k \leqslant 1, \\ & \langle f_{3,\max} \rangle_k \leqslant 1, && k = 1, 2, \cdots, RN \\ & \tilde{\boldsymbol{\gamma}} = \Xi(\boldsymbol{\gamma}) \text{ with the density filter } \Xi, \end{aligned} \tag{15}$$

$$\langle f_{i,\max} \rangle_k = \max(f_{i,e}), \ \text{if} \ \ e \in \Omega \text{ and the } e\text{th element exists}, \ i = 1, 2, 3, \tag{16}$$

where the filtered density of the eth element is $\tilde{\gamma}_e$ and the number of divided sub-domains is RN. The maximum value of the ith constraint functions of the kth subdomain is denoted by $\langle f_{i,\max} \rangle_k$. As the maximum operator is non-differentiable, it is common to choose an approximation function such as the p-norm function, KS function, or a similar function [14,34]. In this research, we used the p-norm approach as follows:

$$\langle f_{i,\max} \rangle_k = c_{i,k}^{iter} \langle f_{i,PN} \rangle_k, \quad (e \in \Omega_k), \tag{17}$$

$$\langle f_{i,PN} \rangle_k \equiv \left(\sum_e (f_{i,e})^p \tilde{\gamma}_e \right)^{1/p}, \quad f_{i,e} \geqslant 0, (e \in \Omega_k), \tag{18}$$

$$c_{i,k}^{iter} = \alpha \frac{f_{i,k,\max}^{iter-1}}{\langle f_{i,PN} \rangle_k^{iter-1}} + (1 - \alpha) c_{i,k}^{iter-1}, \quad 0 < \alpha < 1. \tag{19}$$

In the above equations, the p-norm criterion is multiplied by the correction parameter, $c_{i,k}^{iter}$, determined as the ratio of the value of the p-norm criterion to the value of the maximum constraint function of the previous iteration with a damping parameter, α, to avoid oscillations of the constraints [14,34]. For the p-norm criterion, it is important to note that the value of $f_{i,e}$ should be positive to accurately approximate the maximum value. The first fatigue constraint, $f_{1,e}$, does not present any problems as it is always positive, but the second and third constraints are not always positive depending on the value of mean stress. Thus, simple application of the p-norm criterion to the second and the third constraints is not possible. Furthermore, the failure criterion becomes non-differentiable with the signed von Mises measure [41]. We present our solutions to these problems in Section 2.3.

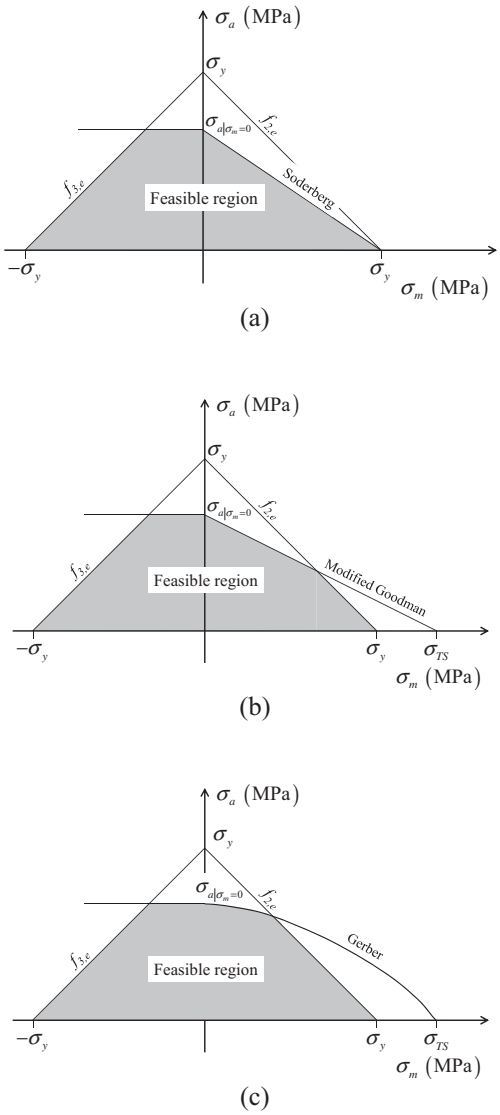

Fig. 4. Failure envelopes of the constraints of the present optimization formulation (14).

2.5. Development of differentiable fatigue failure criteria

2.5.1. Maximum, minimum, and logical *if* operators

As explained in the preceding paragraph, the three explicit fatigue constraints, namely the Gerber, modified Goodman, and Soderberg constraints, are non-differentiable with respect to stress components as well as design variables due to maximum, minimum, and logical "*If*" operators. To reformulate these constraints to be differentiable, we first make the signed von Mises criterion differentiable using the mathematical operators proposed in [34]:

$$\Psi_{2,\max}(a,b) = \frac{a+b}{2} + \frac{\sqrt{(a-b)^2+\varepsilon}}{2} \approx \begin{cases} a, & a \geqslant b \\ b, & a < b, \end{cases} \tag{20}$$

$$\Psi_{2,\min}(a,b) = \frac{a+b}{2} - \frac{\sqrt{(a-b)^2+\varepsilon}}{2} \approx \begin{cases} b, & a \geqslant b \\ a, & a < b, \end{cases} \tag{21}$$

where a and b are arbitrary real values. To determine the maximum and minimum principal stresses, the maximum operator and minimum operator for three real variables can be defined as follows [34]:

$$\begin{aligned}\tilde{\Psi}_{3,\max}(a,b,c) &= \tfrac{a}{4}+\tfrac{b}{4}+\tfrac{c}{2}+\tfrac{\sqrt{(a-b)^2+\varepsilon}}{4}+\frac{\sqrt{\left(\frac{a}{2}+\frac{b}{2}-c+\frac{\sqrt{(a-b)^2}}{2}\right)^2+\varepsilon}}{2},\\ &\approx\begin{cases} a,\ a\geqslant b \text{ and } a\geqslant c,\\ b,\ b\geqslant a \text{ and } b\geqslant c,\\ c,\ c\geqslant a \text{ and } c\geqslant b,\end{cases}\end{aligned} \tag{22}$$

$$\begin{aligned}\tilde{\Psi}_{3,\min}(a,b,c) &= \tfrac{a}{4}+\tfrac{b}{4}+\tfrac{c}{2}-\tfrac{\sqrt{(a-b)^2+\varepsilon}}{4}-\frac{\sqrt{\left(c-\frac{a}{2}-\frac{b}{2}+\frac{\sqrt{(a-b)^2}}{2}\right)^2+\varepsilon}}{2},\\ &\approx\begin{cases} a,\ c\geqslant a \text{ and } b\geqslant a,\\ b,\ c\geqslant b \text{ and } a\geqslant b,\\ c,\ a\geqslant c \text{ and } b\geqslant c,\end{cases}\end{aligned} \tag{23}$$

$$\Psi_{3,\max}(a,b,c)=\begin{pmatrix}\tilde{\Psi}_{\max}(a,b,c)+\tilde{\Psi}_{\max}(a,c,b)+\\ \tilde{\Psi}_{\max}(b,a,c)+\tilde{\Psi}_{\max}(b,c,a)+\\ \tilde{\Psi}_{\max}(c,a,b)+\tilde{\Psi}_{\max}(c,b,a)\end{pmatrix}\Big/6, \tag{24}$$

$$\Psi_{3,\min}(a,b,c)=\begin{pmatrix}\tilde{\Psi}_{\min}(a,b,c)+\tilde{\Psi}_{\min}(a,c,b)+\\ \tilde{\Psi}_{\min}(b,a,c)+\tilde{\Psi}_{\min}(b,c,a)+\\ \tilde{\Psi}_{\min}(c,a,b)+\tilde{\Psi}_{\min}(c,b,a)\end{pmatrix}\Big/6, \tag{25}$$

where ε is a small positive value. Similarly, it is also possible to define an approximated absolute operator and an approximated "*if*" operator as follows:

$$\Psi_{abs}(a)=\sqrt{a^2+\varepsilon}, \tag{26}$$

$$\Psi_{if}(a)=\frac{1}{1+e^{-sa}}=\begin{cases}\approx 1 & \text{if } a>0\\ 0.5 & \text{if } a=0\\ \approx 0 & \text{if } a<0\end{cases}\quad s=100\gg 1. \tag{27}$$

2.6. Differentiable signed von Mises criterion

Using the differentiable logic operators described above, the differentiable signed von Mises stress can be approximated as follows:

$$\begin{aligned}\widehat{\sigma}_m^{\text{signed von Mises}} &= \begin{cases}\sigma_m^{\text{von Mises}} & \text{if } |\sigma_{1,m}|>|\sigma_{3,m}|,\\ 0 & \text{if } |\sigma_{1,m}|=|\sigma_{3,m}|,\\ -\sigma_m^{\text{von Mises}} & \text{if } |\sigma_{3,m}|>|\sigma_{1,m}|,\end{cases}\\ &\cong\{\Psi_{if}(|\sigma_{1,m}|>|\sigma_{3,m}|)-\Psi_{if}(|\sigma_{3,m}|>|\sigma_{1,m}|)\}\times\sigma_m^{\text{von Mises}},\\ &\cong\left\{\frac{1}{1+e^{-s\frac{(|\sigma_{1,m}|-|\sigma_{3,m}|)}{\sqrt{(|\sigma_{1,m}|-|\sigma_{3,m}|)^2+\varepsilon}}}}-\frac{1}{1+e^{-s\frac{(|\sigma_{3,m}|-|\sigma_{1,m}|)}{\sqrt{(|\sigma_{1,m}|-|\sigma_{3,m}|)^2+\varepsilon}}}}\right\}\times\sigma_m^{\text{von Mises}},\end{aligned} \tag{28}$$

where $\widehat{\sigma}_m^{\text{signed von Mises}}$ is a differentiable form of the signed von Mises stress, $\sigma_m^{\text{signed von Mises}}$, in Eq. (13). To avoid too large of an exponent in the "*if*" logic operator in Eq. (28), the difference between the maximum and minimum principal stress values is normalized.

2.7. Differentiable fatigue failure criteria

With the above reformulations, the equivalent multiaxial mean stress and alternating stress become differentiable with respect to the stress components. However, deriving the differentiable fatigue failure criterion of Eqs. (9)–(11) using the above differentiable multiaxial mean stress and alternating stress is still an issue. We therefore formulate the following differentiable formulas with respect to the stress components:

$$\text{Differentiable modified Goodman}: L_e^{GM}=\frac{\sigma_a}{\sigma_{a|\sigma_m=0}}+\frac{\Psi_{2,\max}(\widehat{\sigma}_m^{\text{signed von Mises}},0)}{\sigma_{TS}}\leqslant 1, \tag{29}$$

$$\text{Differentiable Gerber}: L_e^{GB} = \frac{\sigma_a}{\sigma_{a|\sigma_m=0}} + \left(\frac{\Psi_{2,\max}(\widehat{\sigma}_m^{\text{signed von Mises}}, 0)}{\sigma_{TS}}\right)^2 \leqslant 1, \tag{30}$$

$$\text{Differentiable Soderberg}: L_e^{SB} = \frac{\sigma_a}{\sigma_{a|\sigma_m=0}} + \frac{\Psi_{2,\max}(\widehat{\sigma}_m^{\text{signed von Mises}}, 0)}{\sigma_y} \leqslant 1. \tag{31}$$

The differentiable modified Goodman, differentiable Gerber, and differentiable Soderberg are positive and denoted by L_e^{GM}, L_e^{GB}, and, L_e^{SB}, respectively. As they are positive, the above criteria defined at every finite element can be aggregated with the help of the fatigue p-norm criterion, $\langle f_{1,\max}\rangle_k$. p-norm formulas for the second and third constraints are developed in the next subsection.

2.7.1. Global p-norm formula for the second and third static failure criteria

As mentioned in Section 2.1, local constraint functions should always be positive to be aggregated with the p-norm criterion. However, static failure criteria of the second and third constraints, $\langle f_{2,\max}\rangle_k$ and $\langle f_{3,\max}\rangle_k$, are not always positive when $(\sigma_a + \sigma_m)/\sigma_y < 0$ and $(\sigma_a - \sigma_m)/\sigma_y < 0$, as shown in Fig. 5.

To address this issue, we adopt a maximum operator with an element-wise static failure constraint and a value of zero:

$$f_{2,e} = \Psi_{2,\max}\left(\frac{\sigma_a + \widehat{\sigma}_m^{\text{signed von Mises}}}{\sigma_y}, 0\right) \leqslant 1, \tag{32}$$

$$f_{3,e} = \Psi_{2,\max}\left(\frac{\sigma_a - \widehat{\sigma}_m^{\text{signed von Mises}}}{\sigma_y}, 0\right) \leqslant 1. \tag{33}$$

Then, the two constraints become positive and the p-norm approach can be employed.

2.7.2. Localized mode issue for FCTO

When using harmonic finite element calculations to calculate stress values for alternating structural loads in stress-based topology optimization, the localized mode issue becomes critical, which is one of the main findings of this study. Several studies have demonstrated artificial vibrations at low density regions due to linear interpolation or low power penalization of the mass matrix [1,36,37]. Consequently, oscillations of the fatigue constraints become severe and stable optimization convergence cannot be guaranteed. To resolve the side-effects of these localized modes, several numerical and theoretical techniques have been developed. To evaluate the effects of these localized modes on the stress calculation, let us consider the structure shown in Fig. 6, which can be regarded as an intermediate topology optimization design. Application of a harmonic force, results in high oscillations of structural displacements at void regions. Due to these oscillations, associated high stress values are inevitably observed (see Fig. 6, center figure). To suppress these artificial stress values, we use a higher value for the penalization factor of mass matrix interpolation with respect to the density design variable; the approach is both simple and robust. As illustrated in Fig. 6 (bottom figure), artificial stress values at the void regions are successfully suppressed using this higher penalization factor.

2.7.3. Sensitivity analysis

To conduct topology optimization using a gradient-based optimizer, the sensitivity values of the objective and constraints function need to be derived. Sensitivity of the objective function (mass usage) with respect to design variables is simple to derive, but it is more complicated to derive the sensitivities of the constraint functions. Shown below is sensitivity analysis performed using the adjoint variable method:

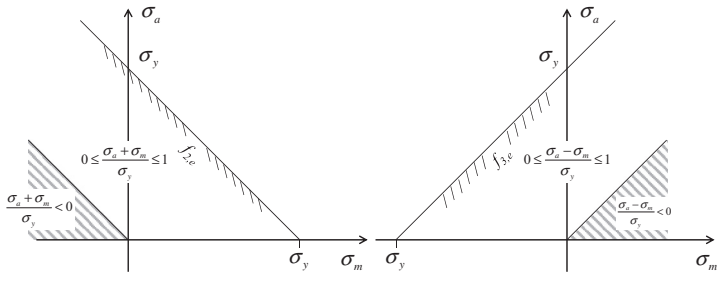

Fig. 5. Static failure envelopes of the present optimization problem.

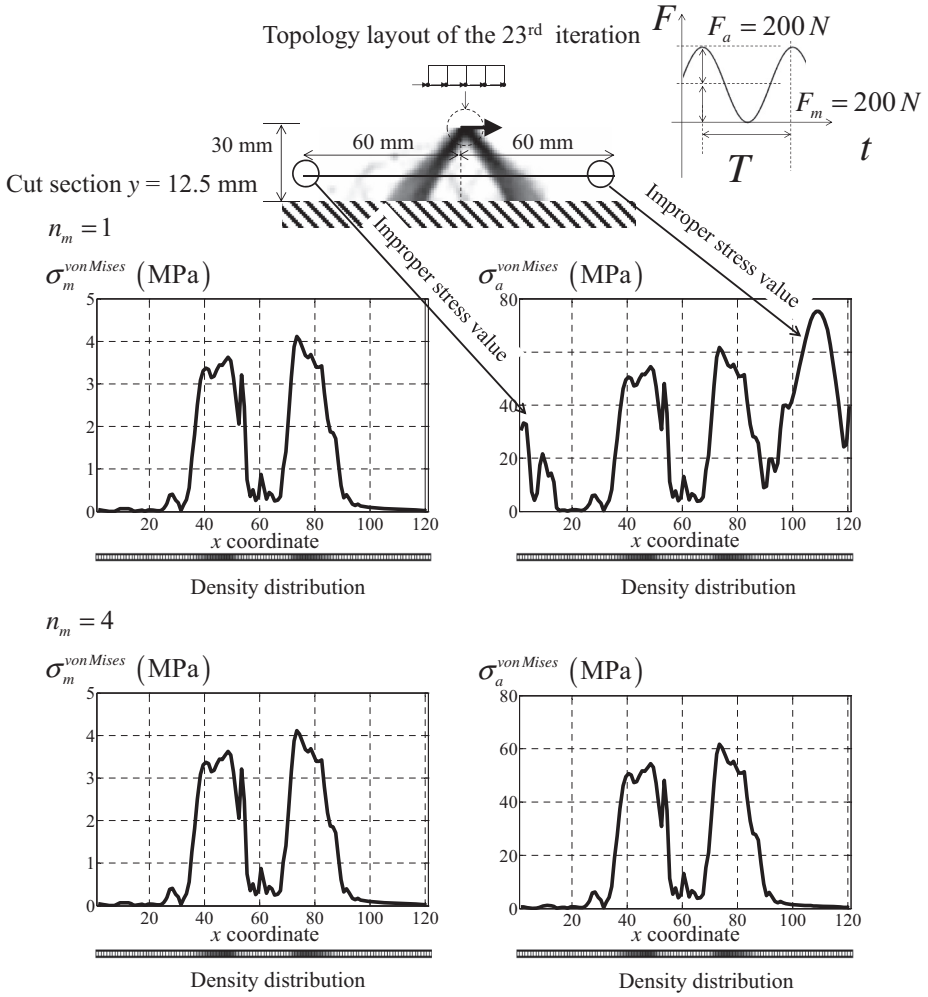

Fig. 6. Localized mode issue.

$$\frac{d\langle f_{i,PN}\rangle_k}{d\tilde{\gamma}_e} = \frac{\partial\langle f_{i,PN}\rangle_k}{\partial\tilde{\gamma}_e} + \frac{\partial\langle f_{i,PN}\rangle_k}{\partial L_{i,e}^{\odot}}\frac{\partial L_{i,e}^{\odot}}{\partial\sigma_a}\frac{\partial\sigma_a}{\partial\boldsymbol{\sigma}_{a,e}}\frac{\partial\boldsymbol{\sigma}_{a,e}}{\partial\tilde{\gamma}_e} + \frac{\partial\langle f_{i,PN}\rangle_k}{\partial L_{i,e}^{\odot}}\frac{\partial L_{i,e}^{\odot}}{\partial\sigma_m}\frac{\partial\sigma_m}{\partial\boldsymbol{\sigma}_{m,e}}\frac{\partial\boldsymbol{\sigma}_{m,e}}{\partial\tilde{\gamma}_e} + \sum_{e'\in\Omega_k}\left(\frac{\partial\langle f_{i,PN}\rangle_k}{\partial L_{i,e}^{\odot}}\frac{\partial L_{i,e}^{\odot}}{\partial\sigma_a}\frac{\partial\sigma_a}{\partial\boldsymbol{\sigma}_{a,e'}}\frac{\partial\boldsymbol{\sigma}_{a,e'}}{\partial\mathbf{U}_a}\frac{d\mathbf{U}_a}{d\tilde{\gamma}_e} + \frac{\partial\langle f_{i,PN}\rangle_k}{\partial L_{i,e}^{\odot}}\frac{\partial L_{i,e}^{\odot}}{\partial\sigma_m}\frac{\partial\sigma_m}{\partial\boldsymbol{\sigma}_{m,e'}}\frac{\partial\boldsymbol{\sigma}_{m,e'}}{\partial\mathbf{U}_m}\frac{d\mathbf{U}_m}{d\tilde{\gamma}_e}\right). \tag{34}$$

Because the external mean and alternating forces are independent of the design variables, the adjoint variables $\boldsymbol{\lambda}_{a,k}^T$ and $\boldsymbol{\lambda}_{m,k}^T$ for the sensitivity analysis can be derived from static equilibrium and dynamic equilibrium equations as follows:

$$\frac{d\mathbf{U}_a}{d\tilde{\gamma}_e} = -\mathbf{K}_a^{-1}\frac{d\mathbf{K}_a}{d\tilde{\gamma}_e}\mathbf{U}_a, \tag{35}$$

$$\frac{d\mathbf{U}_m}{d\tilde{\gamma}_e} = -\mathbf{K}_m^{-1}\frac{d\mathbf{K}_m}{d\tilde{\gamma}_e}\mathbf{U}_m, \tag{36}$$

$$\boldsymbol{\lambda}_{a,k}^T = -\sum_{e'\in\Omega_k}\frac{\partial\langle f_{i,PN}\rangle_k}{\partial L_{i,e}^{\odot}}\frac{\partial L_{i,e}^{\odot}}{\partial\sigma_a}\frac{\partial\sigma_a}{\partial\boldsymbol{\sigma}_{a,e'}}\frac{\partial\boldsymbol{\sigma}_{a,e'}}{\partial\mathbf{U}_a}\mathbf{K}_a^{-1}, \tag{37}$$

$$\boldsymbol{\lambda}_{m,k}^T = -\sum_{e'\in\Omega_k}\frac{\partial\langle f_{i,PN}\rangle_k}{\partial L_{i,e}^{\odot}}\frac{\partial L_{i,e}^{\odot}}{\partial\sigma_m}\frac{\partial\sigma_m}{\partial\boldsymbol{\sigma}_{m,e'}}\frac{\partial\boldsymbol{\sigma}_{m,e'}}{\partial\mathbf{U}_m}\mathbf{K}_m^{-1}, \tag{38}$$

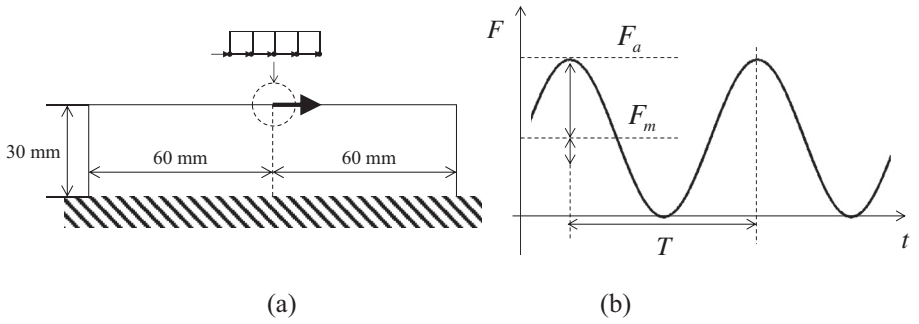

Fig. 7. Design domain, boundary conditions, and loading conditions of the two-bar design problem ($E = 200$ GPa, $v = 0.3$, $\sigma_{TS} = 300$ MPa, $\sigma_y = 165$ MPa, $\rho = 7860$ kg/m^3).

$$\mathbf{K}_a^T \boldsymbol{\lambda}_{a,k} = -\sum_{e' \in \Omega_k} \frac{\partial \langle f_{i,PN} \rangle_k}{\partial L_{i,e}^{\odot}} \left(\frac{\partial L_{i,e}^{\odot}}{\partial \sigma_a} \frac{\partial \sigma_a}{\partial \boldsymbol{\sigma}_{a,e'}} \frac{\partial \boldsymbol{\sigma}_{a,e'}}{\partial \mathbf{U}_a} \right)^T, \tag{39}$$

$$\mathbf{K}_m^T \boldsymbol{\lambda}_{m,k} = -\sum_{e' \in \Omega_k} \frac{\partial \langle f_{i,PN} \rangle_k}{\partial L_{i,e}^{\odot}} \left(\frac{\partial L_{i,e}^{\odot}}{\partial \sigma_m} \frac{\partial \sigma_m}{\partial \boldsymbol{\sigma}_{m,e'}} \frac{\partial \boldsymbol{\sigma}_{m,e'}}{\partial \mathbf{U}_m} \right)^T. \tag{40}$$

Finally, the sensitivity of the constraint function can be derived by applying Eqs. (39) and (40) in Eq. (34) as follows:

$$\begin{aligned} \frac{d\langle f_{i,PN} \rangle_k}{d\tilde{\gamma}_e} &= \frac{\partial \langle f_{i,PN} \rangle_k}{\partial \tilde{\gamma}_e} + \frac{\partial \langle f_{i,PN} \rangle_k}{\partial L_{i,e}^{\odot}} \frac{\partial L_{i,e}^{\odot}}{\partial \sigma_a} \frac{\partial \sigma_a}{\partial \boldsymbol{\sigma}_{a,e}} \frac{\partial \boldsymbol{\sigma}_{a,e}}{\partial \tilde{\gamma}_e} + \frac{\partial \langle f_{i,PN} \rangle_k}{\partial L_{i,e}^{\odot}} \frac{\partial L_{i,e}^{\odot}}{\partial \sigma_m} \frac{\partial \sigma_m}{\partial \boldsymbol{\sigma}_{m,e}} \frac{\partial \boldsymbol{\sigma}_{m,e}}{\partial \tilde{\gamma}_e} \\ &\quad + \boldsymbol{\lambda}_{a,k}^T \frac{d\mathbf{K}_a}{d\tilde{\gamma}_e} \mathbf{U}_a + \boldsymbol{\lambda}_{m,k}^T \frac{d\mathbf{K}_m}{d\tilde{\gamma}_e} \mathbf{U}_m. \end{aligned} \tag{41}$$

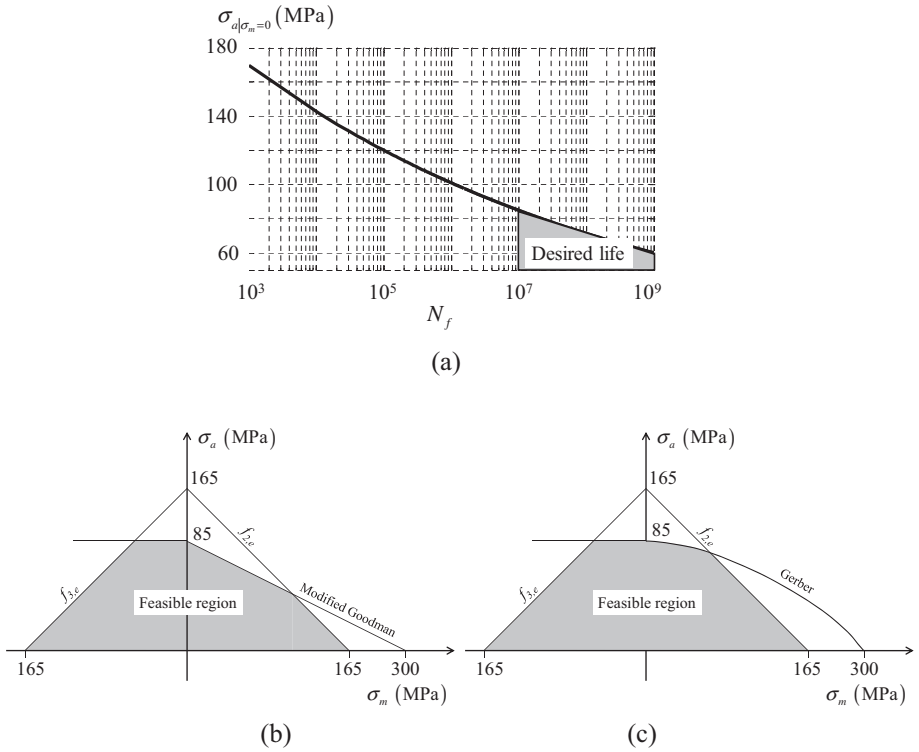

Fig. 8. (a) S-N diagram and failure envelopes of the (b) modified Goodman and (c) Gerber theories (*Basquin* equation: $\sigma_f = 300$ MPa, $b_f = -0.075$, $N_f = 10^7$, therefore $\sigma_{a|\sigma_m=0} \approx 85$ MPa).

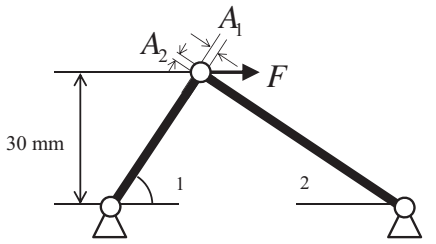

Fig. 9. Size optimization problem of the two-bar structure where the areas and angles of the two bars are the design variables.

3. Topology optimization examples for fatigue constraint

To demonstrate the effectiveness and validity of the present TO method based on the present formulation of Eq. (42), we solve three optimization problems: a two-bar design, a cantilever, and a C-shape bracket. We compare these results with those obtained by size optimization and those reported in the literature. Because the envelopes of the modified Goodman and Soderberg theories are defined by similar formulas with different denominators in Eqs. (9) and (10), we use the modified Goodman theory and Gerber theory to solve fatigue-constrained TO. For stable optimization convergence, we apply density filtering with a fixed filter radius using the Method of Moving Asymptotes as an optimizer [14,34]. The convergence criterion is the largest value of the difference in design variables between sequential iterations. We set the number of maximum iterations to 1000.

$$\begin{aligned} \underset{\boldsymbol{\gamma}}{\text{Minimize}} \quad & V(\boldsymbol{\gamma}) = \sum_{e=1}^{NE} \tilde{\gamma}_e v_e, && (\tilde{\boldsymbol{\gamma}} : \text{Filtered density}) \\ \text{subject to} \quad & \langle f_{1,\max} \rangle_k \leqslant 1, && \\ & \langle f_{2,\max} \rangle_k \leqslant 1, && \\ & \langle f_{3,\max} \rangle_k \leqslant 1, && k = 1, 2, \ldots, RN \\ & \tilde{\boldsymbol{\gamma}} = \Xi(\boldsymbol{\gamma}) \text{ with the density filter } \Xi. && \end{aligned} \tag{42}$$

3.1. Example 1: Two-bar design

For the first optimization example, the two-bar design example shown in Fig. 7 was considered, as relevant STOM studies have used the von Mises Yield criterion or the Drucker–Prager Yield criterion [10]. These previous studies indicated that a structure consisting of two supporting tension and compression bars could be obtained through TO methods by minimizing the volume subject to a static local stress constraint or by minimizing compliance minimization subject to a mass constraint (see [10,17] and references therein). Here, we discretized a rectangular design domain, 120 × 30 mm, using 120 × 30 linear QUAD finite elements. We applied a clamp boundary condition to the bottom line, and evenly applied a fluctuating force (mean force: 200 N, alternating force: 200 N) to the top center five nodes to remove the stress concentration of the external force. In Fig. 7(b), $\mathbf{F}_a$ and $\mathbf{F}_m$ represent the alternating force with a period T and the mean force, respectively. Without loss of generality, the number of sub-regions was set to 4 and the number of total constraints was 12 (4 × 3) using the p-norm approach to fatigue constraints in the optimization formulation (42). Plain carbon steel 1020 was employed; this material has a Young's modulus and Poisson's ratio of $E = 200$ GPa and $\nu = 0.3$, respectively. Ultimate tensile strength (σ_{TS}), yield strength (σ_y), and density (ρ) were set to 300, 165 MPa, and 7860 kg/m^3, respectively. To determine the alternating stress value, $\sigma_{a|\sigma_m=0}$, for a minimum desired number of loading cycles in the S-N diagram in Fig. 8(a), we employed the *Basquin* equation as follows [40,42,43]:

$$\sigma_{a|\sigma_m=0} = \sigma_f (2N_f)^{b_f}. \tag{43}$$

Table 1
Size optimization results of the two-bar size optimization problem.

	Optimal variables by the modified Goodman criterion	Optimal variables by the Gerber criterion
A_1 (mm^2)	2.0147	1.7688
A_2 (mm^2)	1.8054	1.7321
β_1 (deg)	48.136	45.601
β_2 (deg)	41.864	44.399
V_1 (mm^3)	81.158	74.269
V_2 (mm^3)	81.158	74.269

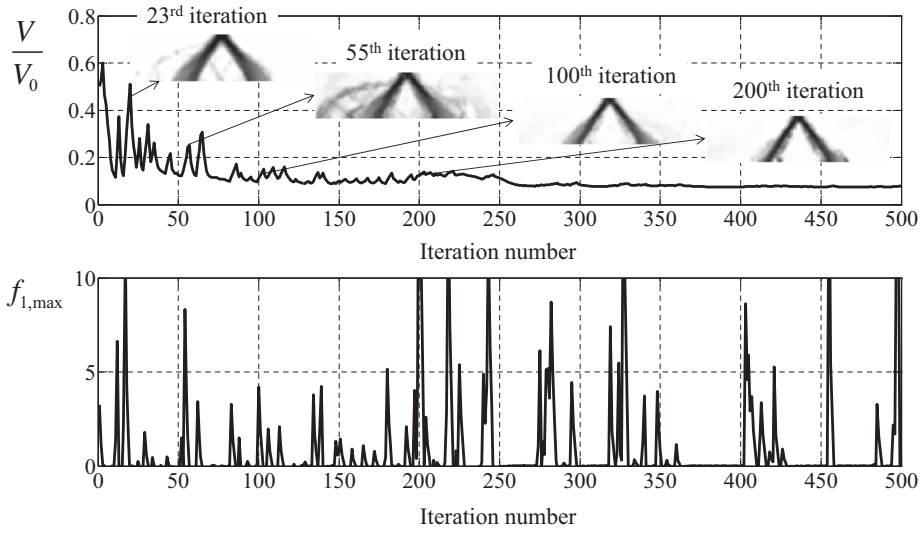

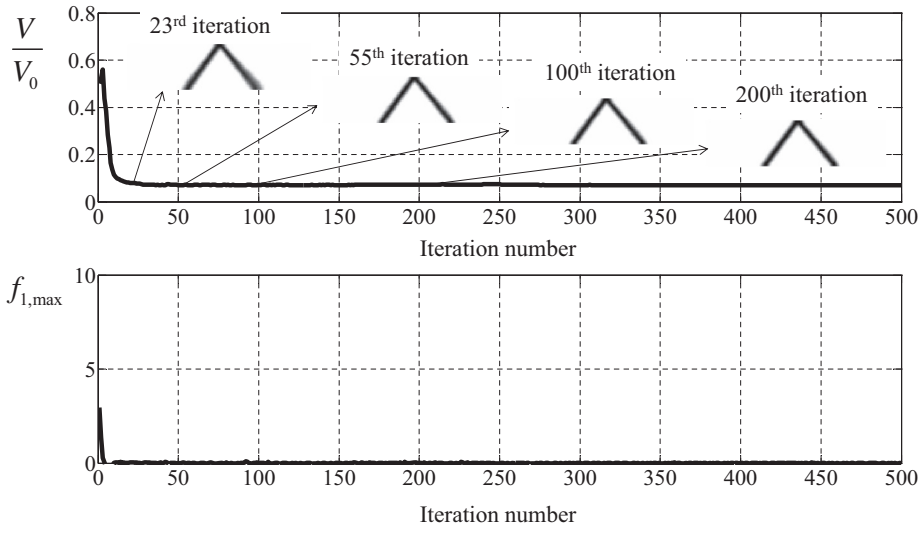

Fig. 10. Localized mode issue: (a) optimization history with the local mode and (b) optimization history without the local mode after application of a higher penalization factor to the mass matrix.

We set the fatigue strength coefficient, σ_f, and the exponent of the *Basquin* equation, b_f, to 300 MPa and −0.075, respectively. The minimum desired number of loading cycles, N_f, was set to 10^7; normally, over 10^6 loading cycles represents an infinite loading cycle. We obtained the failure envelopes of the modified Goodman and Gerber criteria; these are shown in Fig. 8(b, c).

Few studies have considered fatigue constraints in TO. To determine the potential and limitations of the present approach, we first conducted size optimization of the two bars discretized by two truss elements, as shown in Fig. 9. Angles and cross-sectional areas of each bar were set to the design variables of the size optimization problem of minimizing the volume subject to the fatigue failure constraint (the first constraint) and static failure (the second and third constraints) [10].

According to previous relevant research [10], the optimal design variables for size optimization are $\beta_1 = \beta_2 = 45^\circ$ and $A_1 = A = F/\sqrt{2}\sigma_{\max}$, where $\sigma_{\max}$ is the maximum allowable stress value with the same compressive and tensile strength. We performed harmonic finite element analysis as follows:

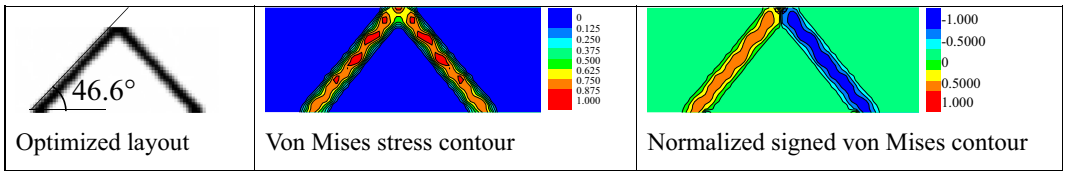

Fig. 11. Topology optimized results of the two-bar structure and their von Mises stress contours: designs with p values of (a) 1.5 ($V(\boldsymbol{\gamma})/V_0 = 0.078$), (b) 2 ($V(\boldsymbol{\gamma})/V_0 = 0.074$), and (c) 4 ($V(\boldsymbol{\gamma})/V_0 = 0.072$).

$$\mathbf{k}_e = \frac{EA_e}{l_e}\begin{bmatrix} c^2 & cs & -c^2 & -cs \\ cs & s^2 & -cs & -s^2 \\ -c^2 & -cs & c^2 & cs \\ -cs & -s^2 & cs & s^2 \end{bmatrix}, \quad \mathbf{m}_e = \frac{\rho A_e l_e}{6}\begin{bmatrix} 2 & 0 & 1 & 0 \\ 0 & 2 & 0 & 1 \\ 1 & 0 & 2 & 0 \\ 0 & 1 & 0 & 2 \end{bmatrix}, \quad \sigma_e = \frac{E}{l_e}[-c \quad -s \quad c \quad s]\mathbf{u}_e, \tag{44}$$

where A_e, l_e, c, and s are the sectional area, length, cosine, and sine of the bar orientation of the eth element, respectively. Then, the size optimization version of Eq. (42) can be formulized as follows:

$$\begin{aligned} \text{Min.} \quad & A_1 l_1 + A_2 l_2 = \left(\tfrac{A_1}{\sin\beta_1} + \tfrac{A_2}{\sin\beta_2}\right) l, \\ \text{subject to} \quad & f_{1,e} = L_e^{(\odot)}(\sigma_a, \sigma_m) \leqslant 1, \\ & f_{2,e} = \tfrac{\sigma_{\max}}{\sigma_y} = \tfrac{\sigma_a + \sigma_m}{\sigma_y} \leqslant 1, \\ & f_{3,e} = -\tfrac{\sigma_{\min}}{\sigma_y} = \tfrac{\sigma_a - \sigma_m}{\sigma_y} \leqslant 1, \qquad e = 1, 2. \end{aligned} \tag{45}$$

In Table 1, optimal solutions to the above formulation based on the modified Goodman criterion and Gerber criterion are presented. Unlike STOM with stress constraints, we obtained asymmetric solutions considering fatigue constraints. Indeed, the structural members were more resistive to compressive load than tensile load; the β_2 angle was smaller than the β_1 angle. This table also shows that the angles optimized by the Gerber criterion tended to be more symmetric because the envelope of the Gerber criterion was larger than that of the modified Goodman criterion. Because the modified Goodman criterion is more conservative than the Gerber criterion, more material is used for the modified Goodman criterion. If a designer wants a more conservative structure, s/he should use the modified Goodman criterion; otherwise, s/he should use the Gerber criterion. Interestingly, when fatigue constraints were considered, the volumes (V_1, V_2) of the left and right bars became equal.

Next, we solved the continuum TO using Eq. (42). Fig. 10 shows optimized layouts obtained using a higher penalization factor than previously used to resolve the local mode issue. As stated, locally vibrating areas were present as a result of the local mode. Indeed, TO with a low mass penalization, n_m, in Eq. (7) could give erratic FEM solutions and optimization convergences, especially for void regions with lower densities. Use of a high mass penalization makes it possible to conduct TO with stable convergence and can help alleviate serious local optima issues based on use of higher penalization factors in the interpolation functions of the stiffness and mass matrices.

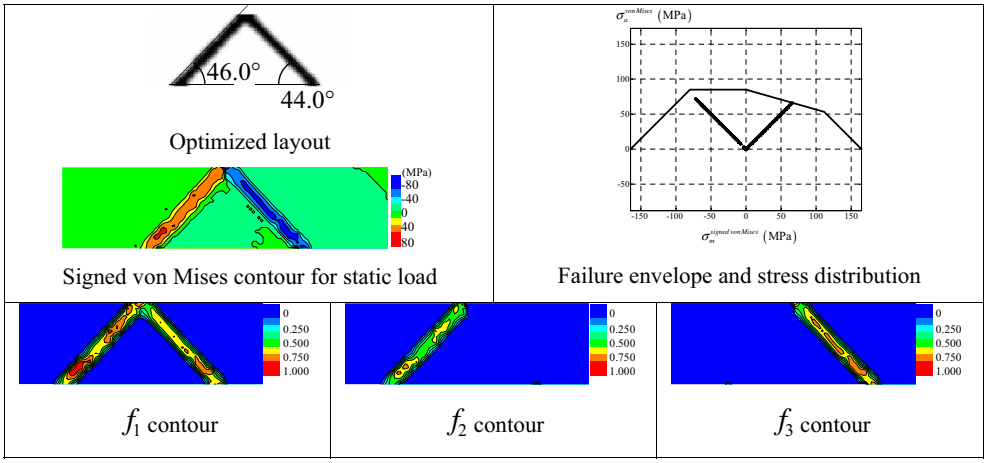

(a)

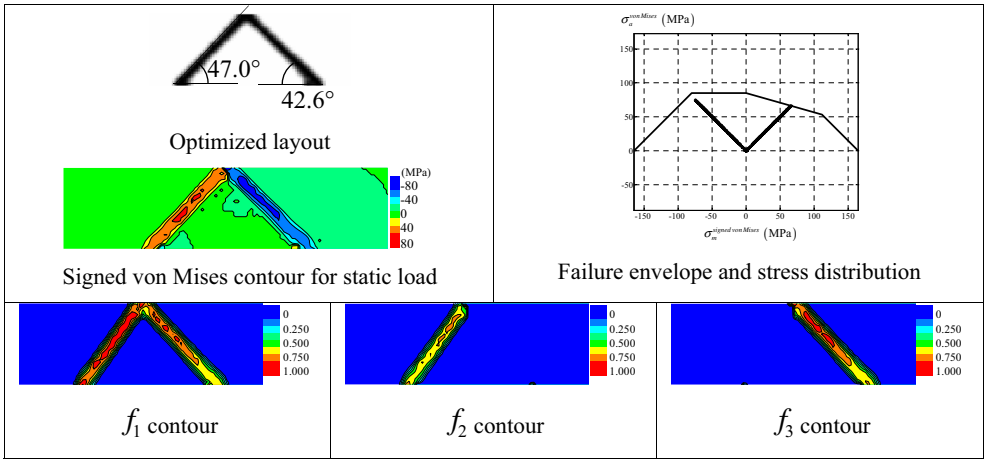

(b)

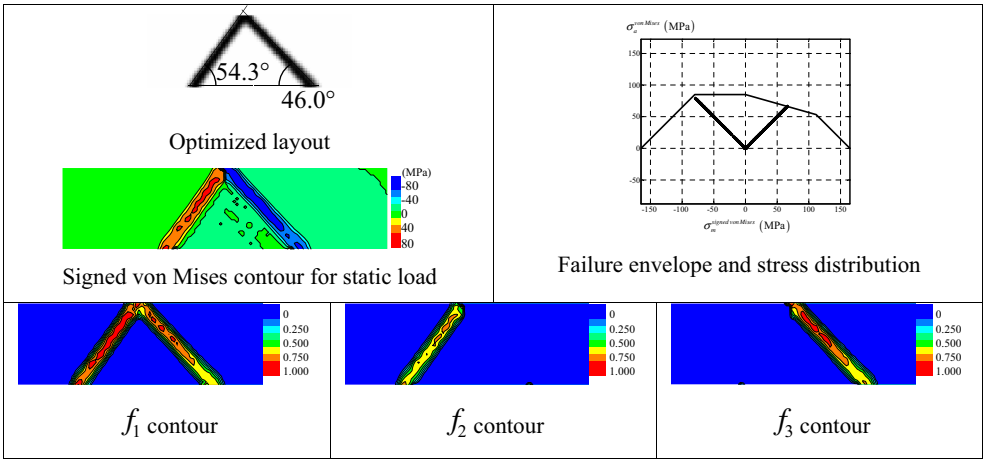

(c)

Fig. 12. Topology optimized results of the two-bar, failure envelope, and three constraints contour considering the modified Goodman criterion: designs with p values of (a) 1.5 ($V(\boldsymbol{\gamma})/V_0 = 0.088$, number of elements with $\widehat{\sigma}_m^{signed\ von\ Mises} > 0$ and $\tilde{\gamma} \geqslant 0.9$, $NE^+ = 80$, number of elements with $\widehat{\sigma}_m^{signed\ von\ Mises} < 0$ and $\tilde{\gamma} \geqslant 0.9$, $NE^- = 82$), (b) 2 ($V(\boldsymbol{\gamma})/V_0 = 0.088$, $NE^+ = 84$, $NE^- = 86$), and (c) 4 ($V(\boldsymbol{\gamma})/V_0 = 0.080$, $NE^+ = 64$, $NE^- = 73$).

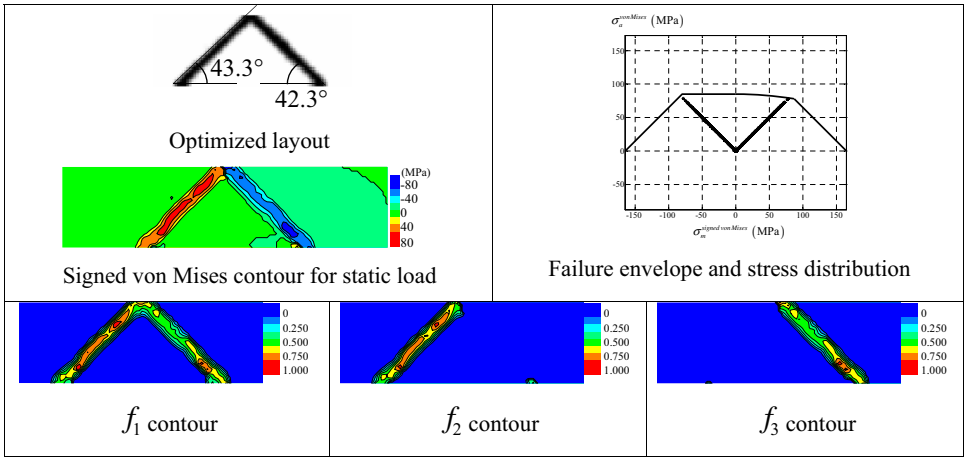

(a)

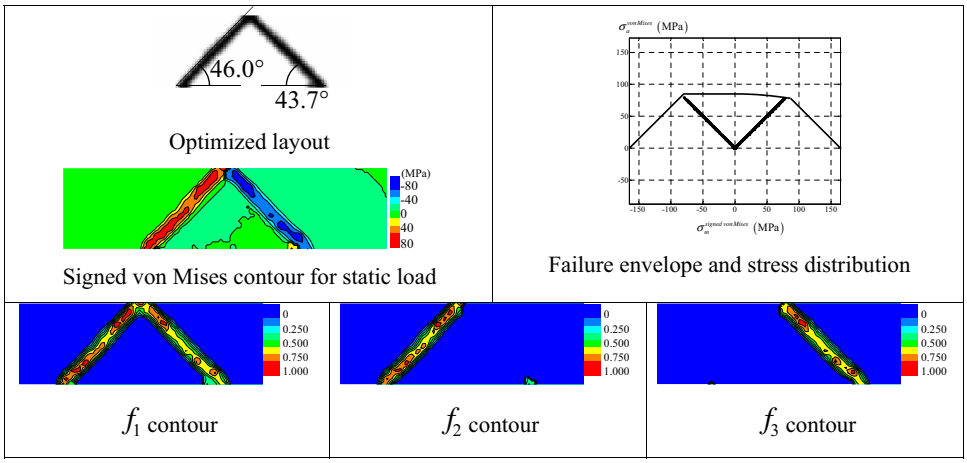

(b)

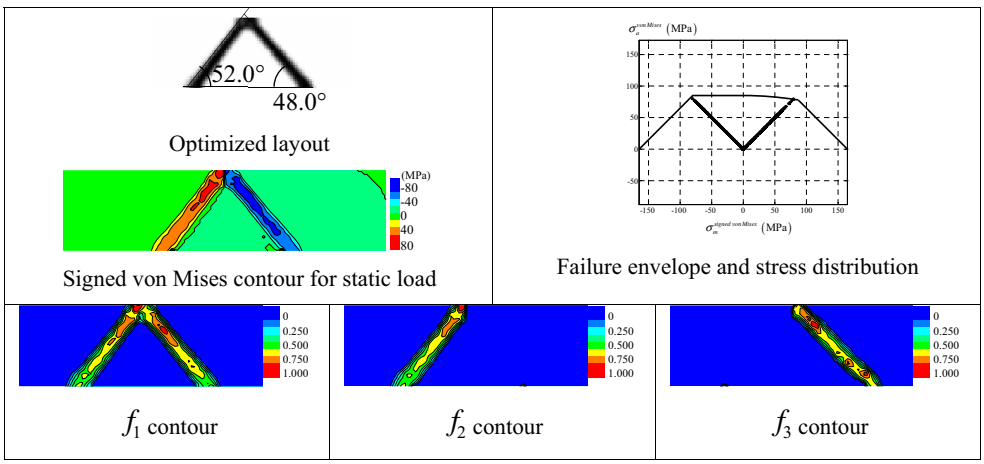

(c)

Fig. 13. Optimized topologies of the two-bar, failure envelope, and three constraints contour considering Gerber criterion: designs with p values of (a) 1.5 ($V(\boldsymbol{\gamma})/V_0 = 0.089$, $NE^+ = 64$, $NE^- = 89$), (b) 2 ($V(\boldsymbol{\gamma})/V_0 = 0.084$, $NE^+ = 60$, $NE^- = 65$), and (c) 4 ($V(\boldsymbol{\gamma})/V_0 = 0.086$, $NE^+ = 67$, $NE^- = 71$).

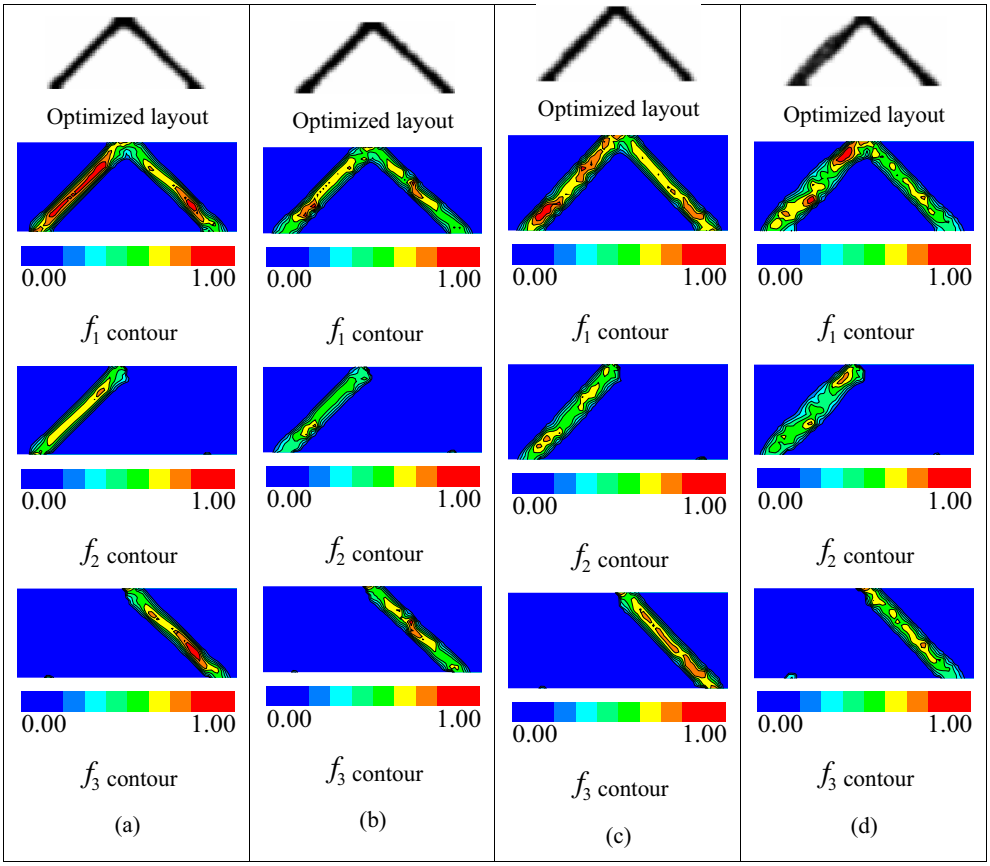

Fig. 14. Optimized layouts for the two-bar with different numbers of sub-domains considering the modified Goodman criterion: (a) 1 sub-domain ($V(\boldsymbol{\gamma})/V_0 = 0.088$), (b) 2 sub-domains ($V(\boldsymbol{\gamma})/V_0 = 0.097$), (c) 4 sub-domains ($V(\boldsymbol{\gamma})/V_0 = 0.088$), and (d) 8 sub-domains ($V(\boldsymbol{\gamma})/V_0 = 0.106$).

Figs. 11–13 show the optimized layouts considering the static failure criteria of the DE theory and the dynamic fatigue failure criteria of the modified Goodman and Gerber theories with different p values, respectively. Comparison of the optimized layouts revealed several important aspects related to fatigue constraints.

First, the unsymmetrical designs shown in Figs. 12 and 13 reflect the influence of the unsymmetrical fatigue constraint in Fig. 8; in contrast, the designs in Fig. 11 based on a static stress constraint are symmetrical, which is linked to size optimization. Unsymmetrical envelopes of dynamic failure criteria have high fatigue strength to compressive load, whereas the DE theory (the static failure criterion) does not distinguish between a compressive load and a tensile load. For a material of

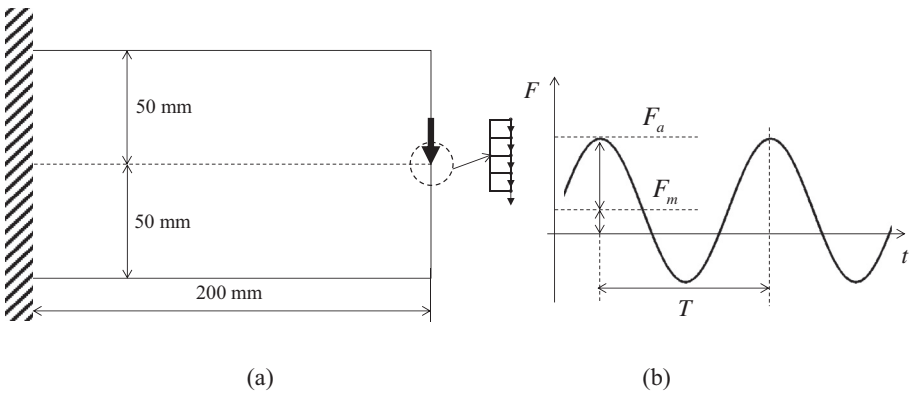

Fig. 15. A cantilever beam structure with mean and alternating forces ($E = 200$ GPa, $v = 0.3$, $\sigma_{TS} = 300$ MPa, $\sigma_y = 165$ MPa, $\rho = 7860$ kg/m^3): (a) geometry and boundary conditions and (b) mean and alternating forces.

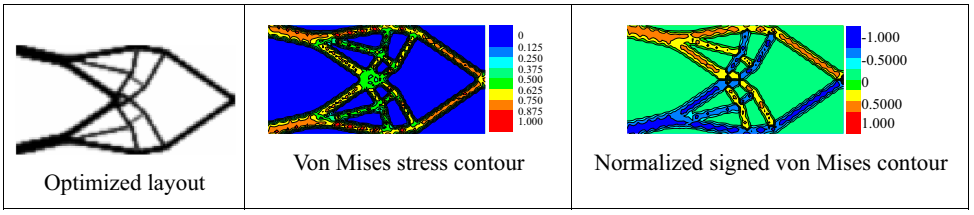

(a)

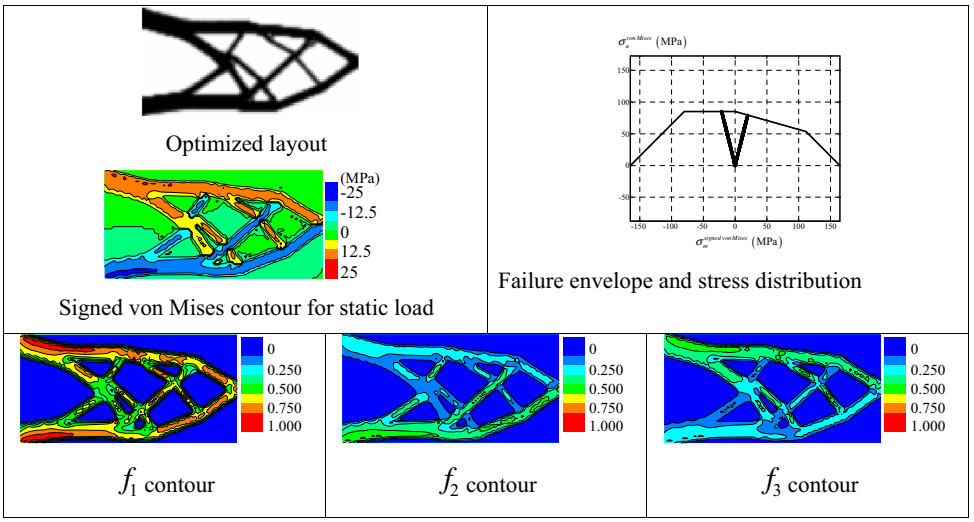

(b)

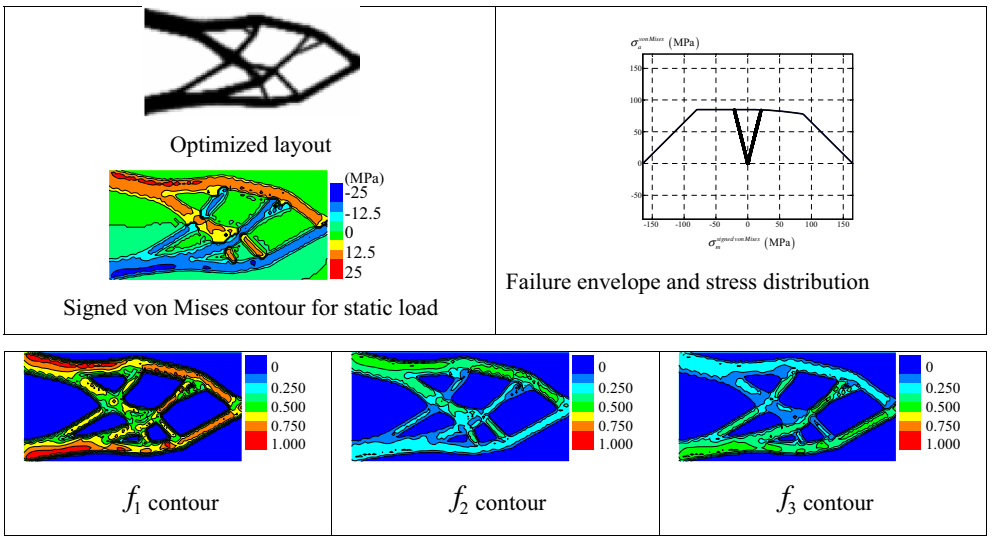

(c)

Fig. 16. Optimized layouts for the cantilever beam ($p = 4$): (a) an optimized layout based on the DE theory (von Mises stress criteria) ($V(\boldsymbol{\gamma})/V_0 = 0.278$), and optimized layouts based on the dynamic fatigue failure of the (b) modified Goodman criterion ($V(\boldsymbol{\gamma})/V_0 = 0.345$, $NE^+ = 570$, $NE^- = 547$) and (c) Gerber criterion ($V(\boldsymbol{\gamma})/V_0 = 0.333$, $NE^+ = 548$, $NE^- = 504$).

interest with a high fatigue strength for a compressive load, unsymmetrical designs, such as those shown in Figs. 12 and 13, are obtained through TO for fatigue constraints. Second, by comparing the optimized layouts in Figs. 11 and 12, and Fig. 13 in terms of angles and volumes with those of the size optimization results shown in Table 1, it is clear that the results obtained with a p value of 1.5 are similar to the size optimization results. To correctly reflect the largest stress value in p norm for a continuum structure, several studies have recommended using a positive integer value of more than 3 for the p value

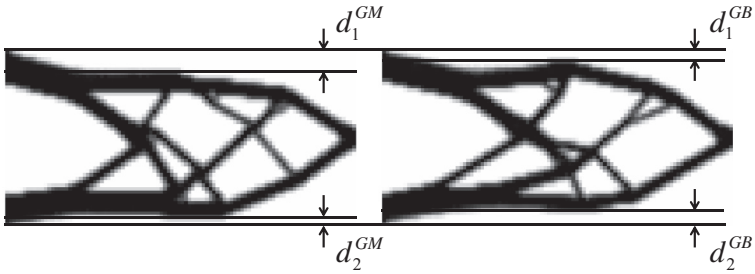

Fig. 17. Comparison of the optimized layouts ($d_1^{GM} > d_2^{GM}, d_1^{GB} \approx d_2^{GB}$).

[14,16,30,34]. Based on our results, we made the following observations with the caveat that the obtained layouts were local optima. The angle between the two bars became narrower as the p value increased. We attribute this to the aggregation characteristics of p-norm. It is likely that a large p value, which plays an important role in aggregating local stress constraints, more severely magnifies the effect of stress concentrations at finite elements near the force and displacement boundary conditions. It is also evident that there were differences between the truss model and the continuum model. In addition, mass ratios with different p values were almost the same in the present examples, where V_0 is the total volume. Third, in the optimized layouts shown in Fig. 12 (modified Goodman) and Fig. 13 (Gerber), the layouts based on the Gerber theory tended to preserve the symmetry property better than those based on the modified Goodman theory. These phenomena can be explained by comparing the shapes of the failure envelopes of the two theories in Fig. 8; the failure envelope of the Gerber theory was more symmetric than that of the modified Goodman theory. Moreover, the volumes of the left and the right bars, NE^+ and NE^-, were similar to each other, as observed in the size optimization results. As a final observation, limitations of the

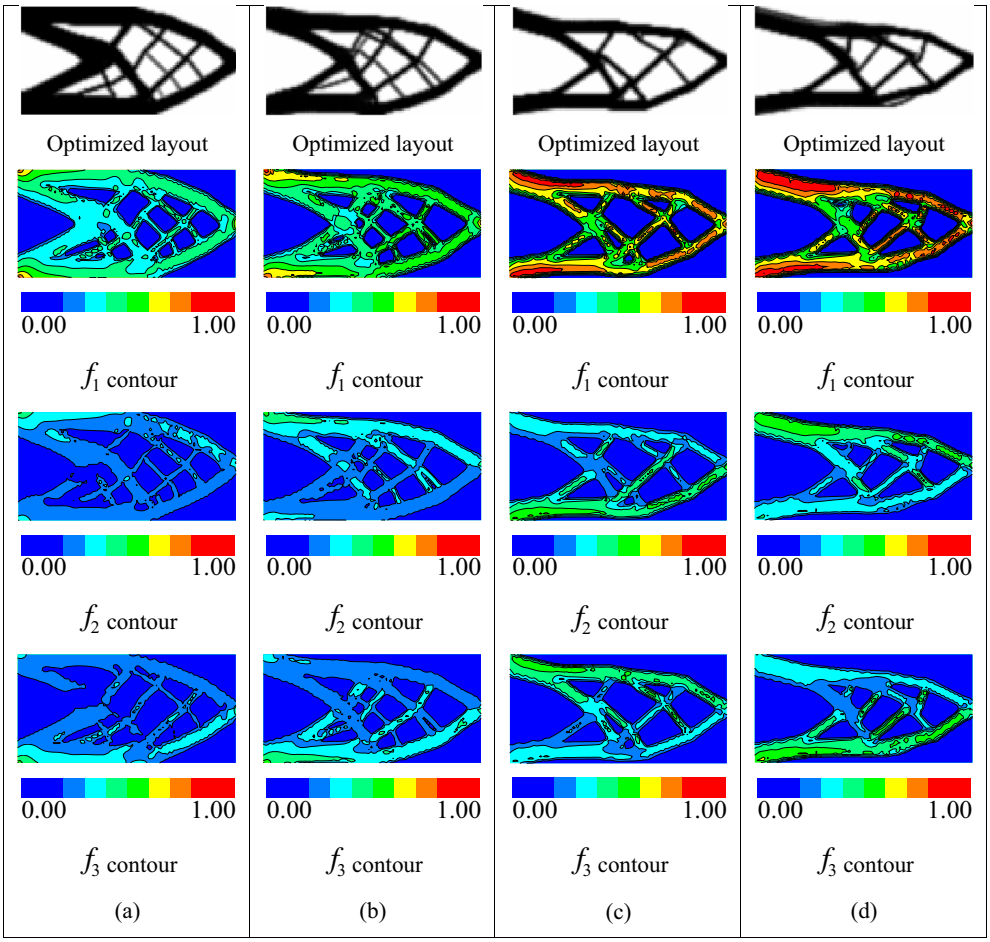

Fig. 18. Optimized layouts for the cantilever beam with different numbers of sub-domains considering the modified Goodman criterion: (a) 2 sub-domains ($V(\boldsymbol{\gamma})/V_0 = 0.540$), (b) 4 sub-domains ($V(\boldsymbol{\gamma})/V_0 = 0.449$), (c) 10 sub-domains ($V(\boldsymbol{\gamma})/V_0 = 0.345$), and (d) 20 sub-domains ($V(\boldsymbol{\gamma})/V_0 = 0.345$).

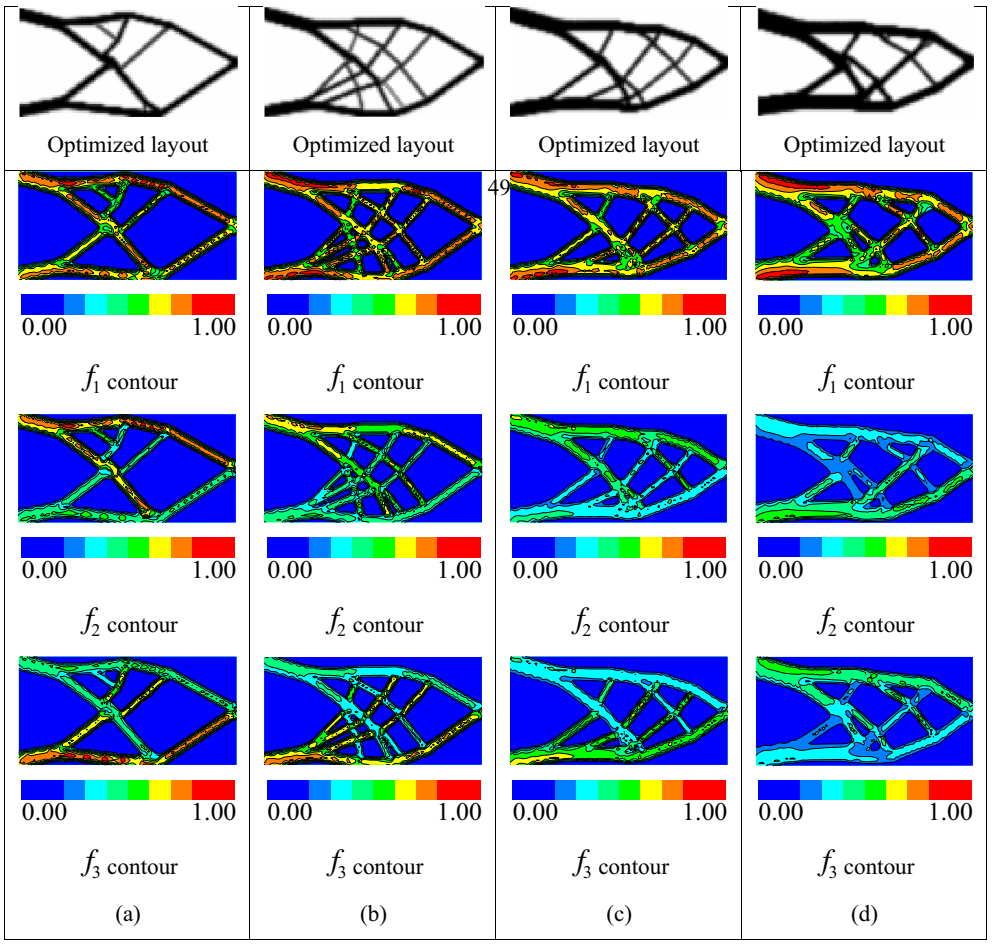

Fig. 19. Optimized layouts for the cantilever beam with different numbers of minimum desired fatigue cycles considering the modified Goodman criterion: minimum of (a) 10^4 ($V(\boldsymbol{\gamma})/V_0 = 0.227$), (b) 10^5 ($V(\boldsymbol{\gamma})/V_0 = 0.256$), (c) 10^6 ($V(\boldsymbol{\gamma})/V_0 = 0.291$), and (d) 10^7 ($V(\boldsymbol{\gamma})/V_0 = 0.345$) desired cycles.

gray elements used in the present approach is evident in the plots of the mean signed von Mises stress and the alternating von Mises stress. Due to use of intermediate design variables for design variable filtering and to address the local optima issues of TO, the stress values of finite elements with lower densities were underestimated. We tested the effect of the number of sub-domains; results are shown in Fig. 14. All optimized results had two bars, but the objective values were different due to the local optimum issue of local constraints.

3.2. Example 2: Cantilever beam

We next considered a cantilever beam structure with a clamped boundary condition and downward proportional loading, as shown in Fig. 15, to evaluate the validity of the observations drawn from the first example. As before, we use the material properties of plain carbon steel 1020 [39]. Design domain was discretized by 5000 2×2 mm quadrilateral Q4 plane stress elements. Number of regions used to calculate p-norm was 10 and the number of constraints in the TO formulation for this example was 30 (10×3). Magnitudes of the mean and 1 Hz alternating forces were set to 100 and 400 N, respectively; it should be emphasized that the forces are proportional loadings. The fatigue strength coefficient, σ_f, and the exponent of the *Basquin* equation, b, were set to 300 MPa and -0.075, respectively. The minimum desired number of loading cycles for the S-N curve, N_f, was set to 10^7.

As in the first TO example, only the static failure criteria of the DE theory and the fatigue failure criteria of the modified Goodman and Gerber theories were used to obtain the optimized layouts and associated stress and constraints contours shown in Fig. 16(a–c). Similar to the observations made in the first TO example, the symmetricity of the optimal layouts was based on the symmetricity of the envelopes of the three constraints. When dynamic fatigue was considered, the tension bars appeared to compensate for fatigue degeneration of the material caused by tensile stress. Second, the layout optimized based on the modified Goodman criterion (Fig. 16(b)) was more unsymmetrical than that of the Gerber criterion (Fig. 16(c)). Moreover, as compared in Fig. 17, the ratio of the upper and lower margins of the cantilever beam (d_1/d_2) was quantitatively larger in Fig. 16(b) than in Fig. 16(c). Additionally, the layout in Fig. 16(b) was more conservative in terms of the used volume

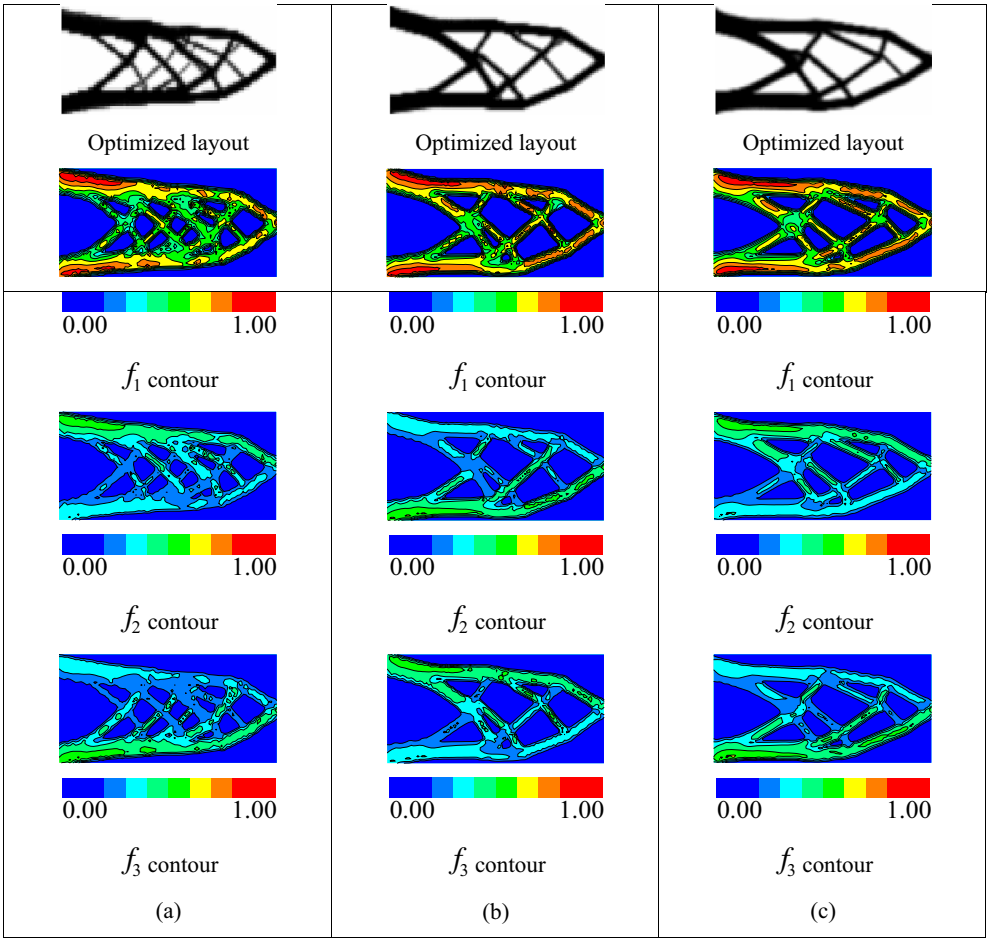

Fig. 20. Optimized layouts for the cantilever beam with different *NE* values considering the modified Goodman criterion: (a) 3200 (80×40) elements ($V(\boldsymbol{\gamma})/V_0 = 0.381$), (b) 5000 ($100 \times 50$) elements ($V(\boldsymbol{\gamma})/V_0 = 0.345$), and (c) 7200 ($120 \times 60$) elements ($V(\boldsymbol{\gamma})/V_0 = 0.363$).

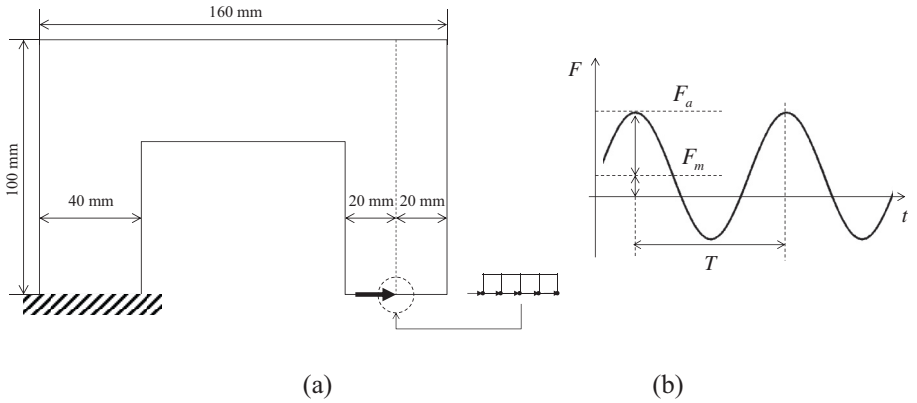

Fig. 21. A bracket with mean and alternating forces ($E = 200$ GPa, $\nu = 0.3$, $\sigma_{TS} = 300$ MPa, $\sigma_y = 165$ MPa, $\rho = 7860$ kg/m^3): (a) geometry and boundary conditions and (b) mean and alternating forces.

than that in Fig. 16(c), because the failure criterion of the modified Goodman is more conservative than that of the Gerber criterion.

Optimized topology layouts obtained by changing the number of sub-domains for the *p*-norm calculation are shown in Fig. 18. Material usage of each optimized layout decreased until the number of sub-domains increased to 20. Use of an appropriate number of sub-domains allowed for effective consideration of the local behavior of the fatigue life constraint, in turn resulting in a better layout with local constraint values evenly distributed in the structural domain. However, it is not clear

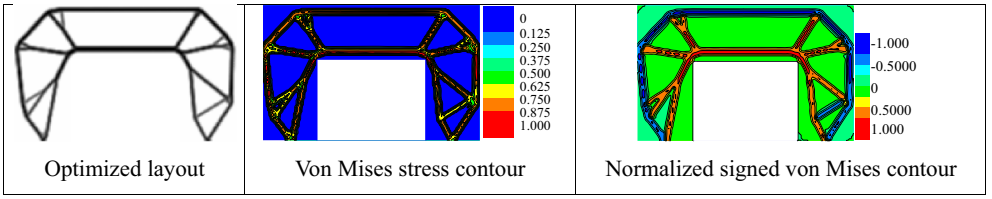

(a)

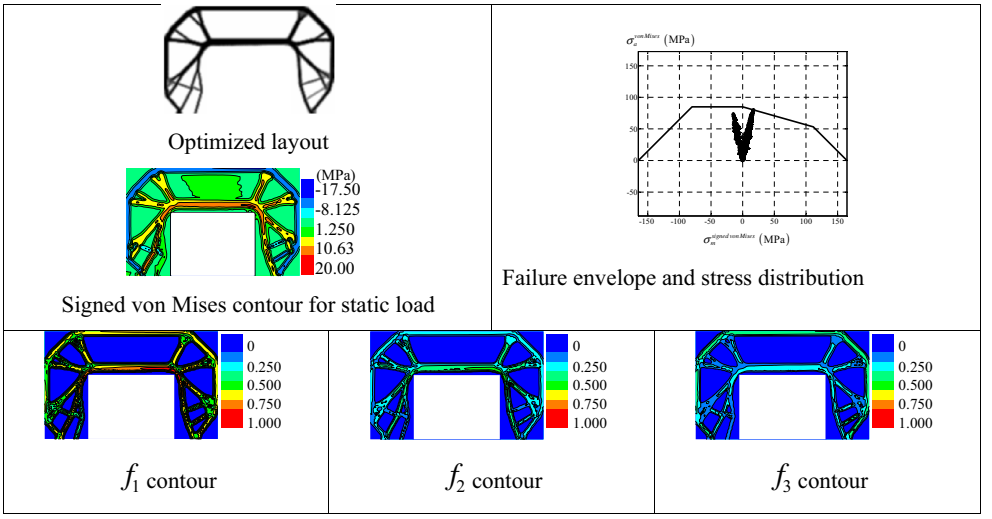

(b)

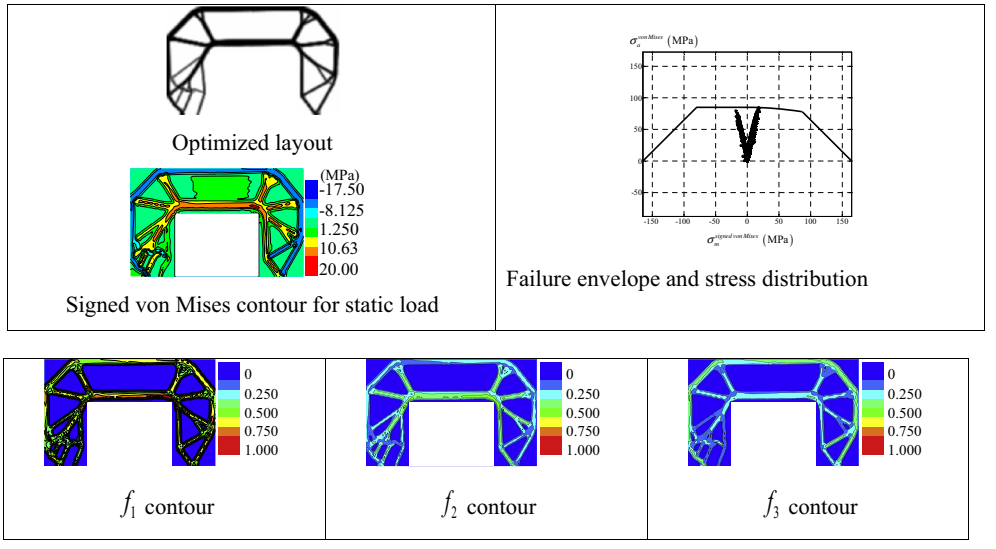

(c)

Fig. 22. Optimized topologies of the bracket: (a) optimized layout considering the von Mises stress criterion ($V(\boldsymbol{\gamma})/V_0 = 0.184$), (b) dynamic fatigue failure based on the modified Goodman criterion ($V(\boldsymbol{\gamma})/V_0 = 0.345$, $NE^+ = 779$, $NE^- = 882$) and (c) Gerber criterion ($V(\boldsymbol{\gamma})/V_0 = 0.295$, $NE^+ = 806$, $NE^- = 885$).

how to choose the number of sub-domains; we proposed values between 4 and 12 for this example based on our numerical experience. In Fig. 19, we show the results of testing the effect of the number of loading cycles. Because an increase in the minimum desired fatigue life resulted in a more conservative fatigue constraint, as expected, the optimized layouts became more conservative with increasing loading cycle number. Fig. 20 shows the effect of the mesh quality on the results. The layouts in Fig. 20(a–c) were obtained with different mesh dimensions (3200 (80×40), 5000 (100×50), and 7200 (120×60)); different layouts were obtained due to the local optima issue. Although we used mesh-independent filtering for this

example, the layouts differed according to changes in mesh size. Because local constraints were considered and regional constraints changed according to the each element's stress or fatigue constraint value, different local optimum were obtained for different mesh sizes.

Example 3: C-shape bracket

For the final optimization example, we chose the C-shape bracket topology optimization problem discretized by 11,200 1×1 mm QUAD elements, as shown in Fig. 21, to determine how our formulation treats reentrant corners. The material properties of plain carbon steel 1020 were used and the same parameter values as used for examples 1 and 2 were assigned to the parameters for the S-N curves. Lower left edge of the bracket was clamped with mean and alternating forces applied at the center part of the right lower edge. Rounded corners are preferred to avoid stress concentration at reentrant corners [14,34]. The number of regions for p-norm was set to 8, and the total number of failure constraints was 24. The magnitudes of the mean and 5 Hz alternating forces were 20 and 100 N, respectively.

Fig. 22(a–c) show the optimized layouts of the bracket constrained using the static failure criterion of the DE theory, the fatigue failure criterion of the modified Goodman theory, and the fatigue failure criterion of the Gerber theory, respectively. Similar to the layout based on the DE theory, the other two layouts had rounded corners at the reentrant domains to avoid stress concentration. Some differences existed at the left clamped edges in Fig. 22(a) and Fig. 22(b, c). The left leg of the two-bar in Fig. 22(a) gathered together at the clamped edge, but several bars emerged in the layouts in Fig. 22(b, c) and were not gathered together, as the fatigue failure criteria was more conservative. This example indicated that rounded corners are preferable not only when considering static failure, but also when considering dynamic failure.

4. Conclusions

Because fatigue failure contributes greatly to the reliability and expected life span of mechanical engineering structures, civil buildings, and marine structures, a mathematical optimization process that considers failures due to static and dynamic loads is an important engineering task. Despite some relevant stress-based topology optimization studies, fatigue failure has rarely been considered in the context of TO. Thus, our focus in the present research was to investigate the effects of local mode and the non-differentiability of fatigue constraints and present some engineering resolutions to these issues to enable successful fatigue constraint TO.

To estimate the fatigue life or the limit number of an alternating loading of a material of interest, we utilized a stress-life approach. To consider the effect of mean stress on fatigue, we used the modified Goodman, Soderberg, and Gerber theories after calculating stress values using a static FE procedure and a harmonic FE procedure. In addition, we demonstrated that the local mode issue, which is problematic in the dynamic topology optimization problem, was also a serious problem in the fatigue-constrained TO method. Localized mode resulted in excessive fluctuations of stress values and associated fluctuations in fatigue constraints, which made the optimization process difficult. We resolved this by employing a higher mass penalization factor. Furthermore, we addressed the differentiability issue of fatigue constraints by introducing differentiable local operators. To demonstrate the applicability and validity of our TO formulation, we obtained optimum solutions for 2D continuum structures. Due to the effects of compressive and tensile forces on fatigue life, unsymmetrical designs and rounded corners, which can also prevent static failure, were obtained. In addition, by comparing the optimum solutions for an idealized truss structure, we investigated the effects and local optimum issues associated with the p-norm penalty factor. In short, we developed and evaluated a new dynamic fatigue-constrained topology optimization method.

Acknowledgement

This work was supported by the research fund of Hanyang University (HY-2013).

Appendix A

A.1. Effective stress measures for alternating stress: von Mises stress and Tresca stress

There are several measures for effective multiaxial alternating stress components similar to the von Mises stress, which is obtained based on distortion energy theory, and Tresca stress, which is obtained based on maximum shear stress theory as follows:

$$\sigma_a^{von\,Mises} = \frac{1}{\sqrt{2}}\sqrt{(\sigma_{1a}-\sigma_{2a})^2+(\sigma_{2a}-\sigma_{3a})^2+(\sigma_{3a}-\sigma_{1a})^2}, \tag{46}$$

$$\sigma_a^{tresca} = \tau_{\max} = \frac{\sigma_{1a}-\sigma_{3a}}{2}, \tag{47}$$

where σ_{1a}, σ_{2a}, and σ_{3a} are the sorted alternating principal stresses. The von Mises stress measure and the Tresca stress measure are denoted by $\sigma_a^{von\,Mises}$ and σ_a^{tresca}, respectively.

A.2. Effective stress measures for mean stress: von Mises stress and hydrostatic axial stress

Similar to the alternating stress criteria, the von Mises criterion can be used for effective multiaxial mean stress as follows:

$$\sigma_m^{von\,Mises} = \frac{1}{\sqrt{2}}\sqrt{(\sigma_{1m}-\sigma_{2m})^2+(\sigma_{2m}-\sigma_{3m})^2+(\sigma_{3m}-\sigma_{1m})^2}, \tag{48}$$

$$\sigma_m^{tresca} = \tau_{\max} = \frac{\sigma_{1m}-\sigma_{3m}}{2}, \tag{49}$$

where σ_{1m}, σ_{2m}, and σ_{3m} are the sorted mean principal stresses. Because these two criteria are always positive, whether an element is under compression or tension cannot be determined. In addition to the above von Mises mean stress measure, the sum of the hydrostatic axial stresses can be used to calculate the effective multiaxial mean stress as follows:

$$\sigma_m^h = \sigma_{1m}+\sigma_{2m}+\sigma_{3m} = \sigma_{xm}+\sigma_{ym}+\sigma_{zm}. \tag{50}$$

References

[1] M.P. Bendsøe, O. Sigmund, Topology Optimization: Theory, Methods, and Applications, Springer, Berlin; New York, 2003.
[2] E. Holmberg, B. Torstenfelt, A. Klarbring, Global and clustered approaches for stress constrained topology optimization and deactivation of design variables, in: 10th World Congress on Structural and Multidisciplinary Optimization, Orlando, Florida, USA, 2013.
[3] J. Norato, C. Le, A method for fatigue-based topology optimization, in: 10th World Congress on Structural and Multidisciplinary Optimization, Orlando, Florida, USA, 2013.
[4] B. Desmorat, R. Desmorat, Topology optimization in damage governed low cycle fatigue, C.R. Mec. 336 (5) (2008) 448–453.
[5] O. Sigmund, A 99 line topology optimization code written in Matlab, Struct. Multidiscip. Optim. 21 (2) (2001) 120–127.
[6] G.H. Yoon, Maximizing the fundamental eigenfrequency of geometrically nonlinear structures by topology optimization based on element connectivity parameterization, Comput. Struct. 88 (1–2) (2010) 120–133.
[7] G.H. Yoon, J.S. Jensen, O. Sigmund, Topology optimization of acoustic-structure interaction problems using a mixed finite element formulation, Int. J. Numer. Meth. Eng. 70 (9) (2007) 1049–1075.
[8] H. Shim, V.T.T. Ho, S.Y. Wang, D.A. Tortorelli, Level set-based topology optimization for electromagnetic systems, IEEE Trans. Magn. 45 (3) (2009) 1582–1585.
[9] S. Kreissl, K. Maute, Levelset based fluid topology optimization using the extended finite element method, Struct. Multidiscip. Optim. 46 (3) (2012) 311–326.
[10] Y.J. Luo, Z. Kang, Topology optimization of continuum structures with Drucker–Prager yield stress constraints, Comput. Struct. 90–91 (2012) 65–75.
[11] A. Verbart, N. Dijk, L.D. Tin, M. Langelaar, F. Keulen, Effect of design parameterization and relaxation on model responses in topology optimization with stress constraints, in: 9th World Congress on Structural and Multidisciplinary Optimization, Shizuoka, Japan, 2011.
[12] G.Y. Qiu, X.S. Li, A note on the derivation of global stress constraints, Struct. Multidiscip. Optim. 40 (1–6) (2010) 625–628.
[13] J. Paris, F. Navarrina, I. Colominas, M. Casteleiro, Block aggregation of stress constraints in topology optimization of structures, Adv. Eng. Software 41 (3) (2010) 433–441.
[14] C. Le, J. Norato, T. Bruns, C. Ha, D. Tortorelli, Stress-based topology optimization for continua, Struct. Multidiscip. Optim. 41 (4) (2010) 605–620.
[15] J. Paris, F. Navarrina, I. Colominas, M. Casteleiro, Topology optimization of continuum structures with local and global stress constraints, Struct. Multidiscip. Optim. 39 (4) (2009) 419–437.
[16] M. Bruggi, P. Venini, A mixed FEM approach to stress-constrained topology optimization, Int. J. Numer. Meth. Eng. 73 (12) (2008) 1693–1714.
[17] M. Bruggi, On an alternative approach to stress constraints relaxation in topology optimization, Struct. Multidiscip. Optim. 36 (2) (2008) 125–141.
[18] K. Svanberg, M. Werme, Sequential integer programming methods for stress constrained topology optimization, Struct. Multidiscip. Optim. 34 (4) (2007) 277–299.
[19] M. Burger, R. Stainko, Phase-field relaxation of topology optimization with local stress constraints, SIAM J. Control Optim. 45 (4) (2006) 1447–1466.
[20] G. Allaire, F. Jouve, H. Maillot, Topology optimization for minimum stress design with the homogenization method, Struct. Multidiscip. Optim. 28 (2–3) (2004) 87–98.
[21] P. Duysinx, M.P. Bendsoe, Topology optimization of continuum structures with local stress constraints, Int. J. Numer. Meth. Eng. 43 (8) (1998) 1453–1478.
[22] R.J. Yang, C.J. Chen, Stress-based topology optimization, Struct. Optim. 12 (2–3) (1996) 98–105.
[23] G.I.N. Rozvany, Difficulties in truss topology optimization with stress, local buckling and system stability constraints, Struct. Optim. 11 (3–4) (1996) 213–217.
[24] E. Lee, K.A. James, J.R.A. Martins, Stress-constrained topology optimization with design-dependent loading, Struct. Multidiscip. Optim. 46 (5) (2012) 647–661.
[25] K.A. James, E. Lee, J.R.R.A. Martins, Stress-based topology optimization using an isoparametric level set method, Finite Elem. Anal. Des. 58 (2012) 20–30.
[26] M. Bruggi, P. Duysinx, Topology optimization for minimum weight with compliance and stress constraints, Struct. Multidiscip. Optim. 46 (3) (2012) 369–384.
[27] M. Kocvara, M. Stingl, Solving stress constrained problems in topology and material optimization, Struct. Multidiscip. Optim. 46 (1) (2012) 1–15.
[28] J. Paris, S. Martinez, F. Navarrina, I. Colominas, M. Casteleiro, Topology optimization of aeronautical structures with stress constraints: general methodology and applications, P. I. Mech. Eng. G-J Aer. 226 (G5) (2012) 589–600.
[29] Q. Xia, T.L. Shi, S.Y. Liu, M.Y. Wang, A level set solution to the stress-based structural shape and topology optimization, Comput. Struct. 90–91 (2012) 55–64.
[30] X. Guo, W.S. Zhang, M.Y. Wang, P. Wei, Stress-related topology optimization via level set approach, Comput. Meth. Appl. Mech. 200 (47–48) (2011) 3439–3452.
[31] T. Gao, W.H. Zhang, Topology optimization involving thermo-elastic stress loads, Struct. Multidiscip. Optim. 42 (5) (2010) 725–738.
[32] G.D. Cheng, X. Guo, Epsilon-relaxed approach in structural topology optimization, Struct. Optim. 13 (4) (1997) 258–266.
[33] G. Cheng, Z. Jiang, Study on topology optimization with stress constraints, Eng. Optim. 20 (2) (1992) 129–148.
[34] S.H. Jeong, S.H. Park, D.H. Choi, G.H. Yoon, Topology optimization considering static failure theories for ductile and brittle materials, Comput. Struct. 110 (2012) 116–132.
[35] K. Svanberg, The method of moving asymptotes – a new method for structural optimization, Int. J. Numer. Meth. Eng. 24 (2) (1987) 359–373.

[36] Y. Maeda, S. Nishiwaki, K. Izui, M. Yoshimura, K. Matsui, K. Terada, Structural topology optimization of vibrating structures with specified eigenfrequencies and eigenmode shapes, Int. J. Numer. Meth. Eng. 67 (5) (2006) 597–628.
[37] N.L. Pedersen, Maximization of eigenvalues using topology optimization, Struct. Multidiscip. Optim. 20 (1) (2000) 2–11.
[38] M. Bruggi, P. Venini, Eigenvalue-based optimization of incompressible media using mixed finite elements with application to isolation devices, Comput. Meth. Appl. Mech. 197 (13–16) (2008) 1262–1279.
[39] R.G. Budynas, J.K. Nisbett, Shigley's Mechanical Engineering Design, ninth ed., McGraw-Hill, New York, 2011.
[40] S. Suresh, Fatigue of Materials, second ed., Cambridge University Press, Cambridge; New York, 1998.
[41] N.W.M. Bishop, F. Sherratt, Finite Element based Fatigue Calculations, NAFEMS Ltd, UK, 2000.
[42] Y.-L. Lee, M.E. Barkey, H.-T. Kang, Metal Fatigue Analysis Handbook: Practical Problem-Solving Techniques for Computer-Aided Engineering, Butterworth-Heinemann, Waltham, MA, 2012.
[43] J.A. Bannantine, J.J. Comer, J.L. Handrock, Fundamentals of Metal Fatigue Analysis, Prentice Hall, Englewood Cliffs, N.J., 1990.
[44] M.P. Bendsoe, O. Sigmund, Material interpolation schemes in topology optimization, Arch. Appl. Mech. 69 (9–10) (1999) 635–654.